JP0550095

JAERI-Research
2005-002

CORROSION BEHAVIOR OF AUSTENITIC AND FERRITIC/MARTENSITIC STEELS IN OXYGEN - SATURATED LIQUID Pb-Bi EUTECTIC AT 450℃ AND 550℃

February 2005

Yuji KURATA, Masatoshi FUTAKAWA and Shigeru SAITO

日本原子力研究所
Japan Atomic Energy Research Institute

本レポートは，日本原子力研究所が不定期に公刊している研究報告書です。
入手の問合わせは，日本原子力研究所研究情報部研究情報課（〒319-1195 茨城県那珂郡東海村）あて，お申し越しください。なお，このほかに財団法人原子力弘済会資料センター（〒319-1195 茨城県那珂郡東海村日本原子力研究所内）で複写による実費頒布をおこなっております。

This report is issued irregularly.
Inquiries about availability of the reports should be addressed to Research Information Division, Department of Intellectual Resources, Japan Atomic Energy Research Institute, Tokai-mura, Naka-gun, Ibaraki-ken 319-1195, Japan.

© Japan Atomic Energy Research Institute, 2005
編集兼発行　日本原子力研究所

Corrosion Behavior of Austenitic and Ferritic/Martensitic Steels in Oxygen-saturated Liquid Pb-Bi Eutectic at 450℃ and 550℃

Yuji KURATA, Masatoshi FUTAKAWA and Shigeru SAITO

Center for Proton Accelerator Facilities
Tokai Research Establishment
Japan Atomic Energy Research Institute
Tokai-mura, Naka-gun, Ibaraki-ken

(Received January 13, 2005)

Static corrosion tests of various austenitic and ferritic/martensitic steels were conducted in oxygen-saturated liquid Pb-Bi eutectic at 450℃ and 550℃ for 3000h to study the effects of temperature and alloying elements on corrosion behavior in liquid Pb-Bi. Corrosion depth is defined as the sum of the thickness of the oxide film including internal oxidation, the grain boundary corrosion depth and the thickness of the formed ferrite layer. The corrosion depth decreases at 450℃ with increasing Cr content in steels regardless of ferritic/martensitic steels or austenitic steels. Appreciable dissolution of Ni and Cr does not occur in the three austenitic steels at 450℃. The corrosion depth of ferritic/martensitic steels also decreases at 550℃ with increasing Cr content in steels whereas the corrosion depth of austenitic steels, JPCA and type 316ss becomes larger due to ferritization caused by dissolution of Ni at 550℃ than that of ferritic/martensitic steels. An austenitic stainless steel containing about 5%Si exhibits fine corrosion resistance at 550℃ because the protective Si oxide film is formed and prevents dissolution of Ni and Cr.

Keywords: Corrosion, Pb-Bi, Accelerator Driven System, Spallation Target, Austenitic Stainless Steel, Si-added Steel, Protective Film, Ferritization, Liquid Metal Penetration

450℃及び550℃の酸素飽和した液体鉛ビスマス中における オーステナイト及びフェライト/マルテンサイト鋼の腐食挙動

日本原子力研究所東海研究所大強度陽子加速器施設開発センター
倉田　有司・二川　正敏・斎藤　滋

（２００５年１月１３日受理）

液体鉛ビスマス中の腐食挙動に及ぼす温度及び合金元素の影響を明らかにするため、450℃及び550℃の酸素飽和した液体鉛ビスマス中で、種々のオーステナイト及びフェライト/マルテンサイト鋼について、3000h の静的腐食試験を実施した。腐食深さを、内部酸化を含む酸化膜の厚さ、結晶粒界腐食深さ、形成したフェライト層の厚さの和と定義した。450℃での腐食深さは、フェライト/マルテンサイト鋼、オーステナイト鋼にかかわらず、鋼材中 Cr 量の増加とともに減少する。450℃では３つのオーステナイト鋼で、Ni 及び Cr の明らかな溶解は起こらなかった。フェライト/マルテンサイト鋼の腐食深さは、550℃でも Cr 量の増加とともに減少する。JPCA 及び 316 ステンレス鋼のオーステナイト系ステンレス鋼の腐食深さは、550℃での Ni の溶解に起因するフェライト化によって、フェライト/マルテンサイト鋼より大きくなる。約 5%の Si を含むオーステナイト系ステンレス鋼は、保護的な Si 酸化膜が形成し、Ni 及び Cr の溶解を防ぐため、550℃で優れた耐食性を示す。

東海研究所：〒319-1195　茨城県那珂郡東海村白方白根 2-4

Contents

1. Introduction ····· 1
2. Experimental ····· 2
2.1 Specimens ····· 2
2.2 Corrosion Test Apparatus and Procedure ····· 3
3. Results and Discussion ····· 3
3.1 Microstructure Observation by an Optical Microscope ····· 3
3.2 EDX Analysis of Perritic/Martensitic Steels ····· 3
3.3 EDX Analysis of Austenitic Stainless Steels ····· 4
3.4 Characteristic of Corrosion in Liquid Pb-Bi ····· 5
4. Conclusions ····· 7

References ····· 9

目次

1.緒言 ····· 1
2.実験方法 ····· 2
2.1 試験片 ····· 2
2.2 腐食試験装置及び実験手順 ····· 3
3.結果及び考察 ····· 3
3.1 光学顕微鏡観察 ····· 3
3.2 フェライト/マルテンサイト鋼のエネルギー分散 X 線解析 ····· 3
3.3 オーステナイト系ステンレス鋼のエネルギー分散 X 線解析 ····· 4
3.4 液体鉛ビスマス中の腐食の特徴 ····· 5
4.結言 ····· 7

参考文献 ····· 9

This is a blank page.

1. Introduction

High flux neutrons produced by spallation reaction between high energy protons and heavy metals can bring about various possibilities in the field of science and technology [1,2]. Accelerator Driven Systems (ADSs) have been proposed for the purpose of treatment of nuclear wastes [3,4]. The ADSs consist of a proton accelerator, a spallation target and a subcritical core. Liquid Pb-Bi eutectic is a potential candidate of the target and coolant. Since the solubility of main elements of structural materials is high in liquid Pb-Bi [5,6], the liquid metal has corrosive properties. Therefore, corrosion tests of the structural materials in liquid Pb-Bi have been actively performed [7-16]. The long-term study on reactors using liquid Pb alloys as a coolant has been conducted in Russia, and technologies and knowledge on liquid Pb alloys have been accumulated [5,7,8]. Experiments have also been conducted using new Pb-Bi loops and corrosion test apparatuses fabricated on the basis of knowledge obtained in Russia.

In previous Russian studies [5,7,8], importance of oxygen control in liquid Pb-Bi was pointed out and martensitic steels containing Si were developed for corrosion resistance. From the viewpoints of material corrosion it is important to know what kind of corrosion phenomenon occurs in liquid Pb-Bi. Phenomena such as oxidation, dissolution, precipitation, grain boundary corrosion, mass transfer, erosion and penetration of Pb-Bi into steels occur in liquid Pb-Bi. Furthermore, the phenomenon of ferritization of the austenitic steels owing to Ni dissolution was reported [11,16].

Recently, new experimental results on corrosion in liquid Pb-Bi were reported[17-28]. Mueller et al.[17] conducted corrosion tests of AISI 316L and 1.4970 austenitic stainless steels and 10%Cr martensitic steel up to 7200h in flowing liquid Pb-Bi. These steels exhibited corrosion resistance up to 550℃ if 10^{-6}% oxygen was dissolved in the liquid Pb-Bi. They guessed that the oxygen concentration was low at some parts suffering from dissolution attack. Severe corrosion attack occurred at 600℃. Aiello et al.[18] performed corrosion tests of AISI 316L and T91(Mod.9Cr-1Mo steel) in flowing liquid Pb-Bi with low oxygen concentration ($Co=10^{-8}$-10^{-10} wt%) and high oxygen concentration ($Co=10^{-5}$-10^{-6} wt%) at 400℃. Gomez-Briceno et al.[19], Soler et al.[20] and Martin et al.[25] conducted corrosion tests in static liquid Pb-Bi with different oxygen concentrations and exhibited that dissolution occurred under reducing environment with low oxygen concentrations. Furthermore, they studied stability of the oxide layer formed in liquid Pb-Bi and indicated the existence of threshold temperature above which the formation of a protective and stable oxide layer was not possible. The threshold temperature seemed to depend on material composition, oxygen concentration in liquid Pb-Bi. Gnecco et al.[22] carried out corrosion tests of AISI 316L and T91 in

static liquid Pb-Bi at 550℃ and showed formation of oxide layers under high oxygen condition and penetration of Pb and Bi under low oxygen condition. Furukawa et al.[23,24] examined corrosion behavior of ODS steel, 12%Cr steel and 316ss in static Pb-Bi at 500 to 650℃. Ilincev et al.[27] performed corrosion tests of 20 types of structure steels using thermal convection loops with flowing Pb-Bi at 500 and 400℃, and with different oxygen concentrations.

Corrosion tests using liquid Pb-Bi loop are conducted to study flow rate effect, erosion and mass transfer caused by dissolution at high temperature parts and precipitation at low temperature parts. Phenomena such as oxidation, dissolution, grain boundary corrosion, penetration of Pb-Bi and ferritization can be also investigated in static corrosion tests whose purposes are understanding of basic corrosion mechanism and screening of materials. It is essential to make a corrosion map in liquid Pb-Bi in order to understand the corrosion behavior and use the liquid metal as target and coolant of ADSs. The corrosion map will show what corrosion phenomena and what extent of corrosion damage occur under various liquid Pb-Bi conditions. Parameters for the corrosion map are temperature, temperature gradient at high temperature parts and low temperature parts, alloying elements in steels, oxygen concentration in liquid Pb-Bi, flow rate, irradiation, etc. Equipments and the first R & D program for the corrosion map are described in Ref. [12].

In this study, effects of temperature and contents of alloying elements, Cr, Ni and Si in steels on corrosion behavior are investigated using a static corrosion apparatus for the purpose of drawing the corrosion map. The fact that an austenitic stainless steel containing 5%Si has the excellent corrosion resistance has been published as a part of the results obtained in this study[28].

2. Experimental

2.1 Specimens

Table 1 shows chemical compositions of materials used in the experiment. F82H, Mod.9Cr-1Mo steel, 410ss, 430ss and 2.25Cr-1Mo steel are ferritic/martensitic steels. The 14Cr-16Ni-2Mo steel(JPCA), 316ss and SX (Trademark of the Sandvik Corporation) are austenitic stainless steels. The SX steel is an alloy developed for use in a sulfuric acid environment and the characteristic of the steel is high Si content. The size of corrosion specimens was 15mm x 30mm x 2mm, and a hole of 7.2mm diameter for installation was made at the top of the specimen. Corrosion specimens were polished using emery papers up to #600.

2.2 Corrosion test apparatus and procedure

Fig.1 shows a schematic diagram of a corrosion test apparatus in liquid Pb-Bi. The static corrosion test apparatus was described in detail elsewhere [12]. Components contacting liquid Pb-Bi were made of quartz in the corrosion equipment. As received eutectic Pb-Bi (45Pb-55Bi) of 7kg was used in the present test. The chemical composition of the Pb-Bi was the following:55.60Bi-0.0009Sb-0.0002Cu-0.0001Zn-0.0005Fe-0.0007As-0.0005Cd-0.0001Sn-Bal.Pb(wt%). The Pb-Bi was melted in a pot under Ar gas environment. Ar gas of 99.9999% purity was used as a cover gas over the liquid Pb-Bi. Corrosion tests were conducted at 450℃ and 550℃ for 3000h. PbO was formed on the surface of the liquid Pb-Bi and corrosion tests were made in oxygen-saturated liquid Pb-Bi. Oxygen saturation concentration was estimated to be 3.2×10^{-4} wt% at 450℃ and 1.2×10^{-3} wt% at 550℃ using the equation in the literature [5].

Test specimens were cleaned in silicone oil at about 170℃ after the corrosion tests to remove Pb-Bi stuck to the surface of the specimens. However, there was adherent Pb-Bi left on some parts of the specimen surface. Analyses were made using an optical microscope and a scanning electron microscope (SEM) with energy dispersion X-ray (EDX) for the specimen plated with copper to protect corrosion films during polishing. X-ray diffraction was also used to characterize corrosion products.

3. Results and Discussion

3.1 Microstructure observation by an optical microscope

Figs.2 and 3 show optical micrographs of the cross sections of specimens after corrosion in liquid Pb-Bi for 3000h at 450℃ and 550℃, respectively. Grey corrosion films are observed under copper plating. The adherent Pb-Bi left on some parts of the specimen surface is also recognized, for example, in Fig.2(b). Curving and peeling of corrosion films are observed in Fe whose corrosion films are thick as shown in Fig.2(g) and Fig.3(g). There is a ferrite layer mentioned later near the surface region of JPCA and 316ss after corrosion at 550℃ for 3000h in Figs.3 (c) and (h). Formation of the ferrite layer was not observed in the specimens of JPCA, 316ss and SX after corrosion at 450℃ and in the SX specimen after corrosion at 550℃. Furthermore, the grain boundary corrosion mentioned in 3.4 was observed in F82H, Mod.9Cr-1Mo steel, 410ss, 430ss and 2.25Cr-1Mo steel.

3.2 EDX analysis of ferritic/martensitic steels

The results for EDX analysis of Mod.9Cr-1Mo steel after corrosion at 450℃ and 550℃ are shown in Figs 4 and 5, respectively. It is found that the corrosion film is

oxide of Fe and Cr from the elements mapping. Fig.4 shows that double layer oxides are formed: the outer corrosion film is a fragile iron oxide and the inner corrosion film is Cr-Fe spinel. This result agrees with the result that outer magnetite and inner Cr-Fe spinel were formed during corrosion in liquid Pb-Bi[12, 15]. An internal oxidation layer(oxygen diffusion layer)[17, 19, 23] described in 3.4 is observed under the Cr-Fe spinel at 550℃ in Fig.5.

Figs.6, 7 and 8 show the results for EDX analysis of type 410ss after corrosion in liquid Pb-Bi at 450℃ and 550℃. As shown in Figs.6 and 8, a thin oxide layer was formed on the surface of the steels during the exposure to liquid Pb-Bi. The line analysis in Fig.7 indicates that the thin oxide layer is composed of O, Cr and Fe.

Figs.9, 10 and 11 show the results for EDX analysis of 2.25Cr-1Mo steel after corrosion in liquid Pb-Bi at 450℃ and 550℃. The results for EDX analysis of 2.25Cr-1Mo steel are similar to those for Mod.9Cr-1Mo steel. Fig.10 shows the result of line analysis for 2.25Cr-1Mo steel after corrosion in liquid Pb-Bi at 450℃ for 3000h. The outer corrosion film of iron oxide is porous and fragile because Pb and Bi penetrate into the outer magnetite and reach the Cr-Fe spinel surface. There is no more penetration of Pb and Bi into the spinel layer. This result agrees with that observed by Mueller et al.[17].

3.3 EDX analysis of austenitic stainless steels

The results for EDX analysis of JPCA after corrosion at 450℃ and 550℃ are shown in Figs 12 and 13, respectively. No decrease in Cr, Ni and Fe concentrations near the surface region in Fig.12 means that appreciable dissolution of these elements into liquid Pb-Bi did not occur at 450℃. On the other hand, Fig.13 shows the formation of the layer with excessive decrease in Ni and Cr under the corrosion film for JPCA at 550℃. Enrichment of O, Cr and Fe is observed in the corrosion film. Furthermore, Pb and Bi penetrate deeply into the layer with depletion of Ni and Cr.

Figs.14, 15 and 16 show the results for EDX analysis of type 316ss after corrosion at 450℃ and 550℃. Similar results between JPCA and 316ss were obtained. As indicated in Figs.15 and 16, the ferrite layer with depletion of Ni and Cr is formed beneath the oxide layer. The oxide layer on the surface of 316ss seems to be Cr-Fe spinel. Pb and Bi penetrate into the ferrite layer.

Figs.17, 18 and 19 show the results for EDX analysis of SX after corrosion at 450℃ and 550℃. A corrosion film on SX at 450℃ is very thin and decrease in Cr, Ni and Fe concentrations is not recognized near the surface(Fig.17). Similarly, appreciable dissolution of Ni and Cr is not observed for SX even after corrosion at 550℃ for

3000h(Fig.18). Fig.19 shows the result of EDX line analysis made with higher magnification. A thin continuous film with the thickness of 200 to 400nm is formed on the surface of the SX specimen. The film is an oxide composed of Si and O. Enrichment of Cr, Fe and Ni is not observed in the oxide film. It is found from the comparison of corrosion behavior among JPCA, 316ss and SX that the thin oxide film on SX prevents ferritization of the austenitic steel because Ni and Cr concentrations keep constant beneath the oxide film.

3.4 Characteristic of corrosion in liquid Pb-Bi

It is considered that phenomena such as oxidation, dissolution, grain boundary corrosion, penetration of Pb-Bi and ferritization can be observed in static corrosion tests depending on materials and corrosion condition. An example of grain boundary corrosion is shown in Fig.20 for 2.25Cr-1Mo steel after corrosion at 550℃ for 3000h. This type of grain boundary corrosion was often observed beneath the surface corrosion film in F82H, Mod.9Cr-1Mo steel, 410ss, 430ss and 2.25Cr-1Mo steel. Fig.21 shows an example of internal oxidation of Mod.9Cr-1Mo steel after corrosion at 550℃ for 3000h. The internal oxidation layer is also called an oxygen diffusion layer[17, 19, 23]. The internal oxidation was found in Mod.9Cr-1Mo steel and F82H after corrosion at 550℃ for 3000h.

One of typical examples of corrosion damage in liquid Pb-Bi is the ferritization of austenitic steels due to dissolution of Ni [11,16]. In this study, the ferritization of JPCA and 316ss occurred in the static corrosion test at 550℃ and Pb and Bi penetrated into the formed ferrite layer. Fig.22 shows a typical example of ferritization of JPCA. Austenitic stainless steels are composed of γ phase with face-centered cubic structure. When the ferritization of the austenitic steels occurs, the part of the steels changes into α phase with body-centered cubic structure. The change is detected by using an X-ray diffraction method. Figs. 23 and 24 indicate the results of X-ray diffraction of JPCA and SX before and after corrosion at 550℃, respectively. It is found that the layer with excessive decrease in Ni and Cr is a ferrite phase because peaks of Fe-Cr ferrite phase(α) are detected on JPCA after corrosion at 550℃ as shown in Fig.23. On the other hand, only peaks of austenite phase(γ) are detected on SX specimen even after corrosion at 550℃ in Fig.24. Benamati et al. [11] showed that the ferritization of austenitic stainless steels, AISI 316L and Mannet II occurred during the static corrosion test under oxygen-saturated Pb-Bi condition at 550℃. Furthermore, Mueller et al. [16] indicated that AISI 316L exhibited dissolution of Ni and penetration of Pb and Bi into the ferrite layer during a loop test at 600℃. Since the austenitic steel did not exhibit

appreciable dissolution of Ni and Cr at 450℃ in this study, the temperature where the ferritization of JPCA and 316ss occurs under oxygen-saturated Pb-Bi condition lies between 450℃ and 550℃. On the other hand, the corrosion film of Si oxide formed on SX in Pb-Bi at 550℃ can prevent dissolution of Ni and ferritization of the austenitic stainless steel. This information is important to draw the corrosion map in liquid Pb-Bi.

It was found that Si oxide without enrichment of Cr, Fe and Ni was formed on SX during corrosion in Pb-Bi at 550℃ in this study. It was reported that Si addition to Fe-9%Cr steel produced a protective SiO_2 layer at the oxide-metal interface and brought about significant improvement of corrosion resistance in a gas environment at 575-650℃ [29]. Benemati et al. [11] also reported that Fe-Cr oxide containing 3%Si was formed in liquid Pb-Bi and kept corrosion resistance as a result of loop tests at 450℃ and 550℃ for 700h for Russian martensitic steel, EP823 [8] containing 2%Si. The fact that thin and dense Si oxide was formed on SX in this study is a little different from the results of formation of Fe-Cr oxides containing Si. Although it is difficult to determine the exact chemical composition of the thin corrosion film on SX from the EDX line analysis shown in Fig.19, the formation of Si oxide without enrichment of Cr, Fe and Ni is recognized. As shown in Figs.4, 5, 9, 10 and 11, the outer magnetite and the inner Cr-Fe spinel oxide were formed on Mod.9Cr-1Mo steel and 2.25Cr-1Mo steel. It is considered that Cr-Fe spinel oxide was formed on JPCA and 316ss because enrichment of O, Cr and Fe was detected in the corrosion film. The thin oxide film on SX is different from magnetite and Cr-Fe spinel oxide. Figs. 23 and 24 clearly show occurrence of the ferritization on the JPCA steel and prevention of the ferritization on the SX steel.

From the above-mentioned results it is considered that the oxide of Fe and Cr did not play an effective role as a diffusion barrier of Ni and Cr at 550℃. However, the film of Si oxide formed on SX during corrosion at 550℃ exhibits an effective role as a diffusion barrier of Ni and Cr. The experimental results obtained by Martin et al.[25] pointed the existence of the threshold temperature above which formation of a protective oxide layer was not possible in liquid Pb-Bi. The threshold temperature depended on materials, corrosion condition and time. Magnetite and Cr-Fe spinel formed on JPCA and 316ss in oxygen-saturated liquid Pb-Bi at 550℃ are not protective, in particular for diffusion of Ni and Cr. Therefore, it is necessary to find and develop corrosion-resistant steels with a protective oxide layer such as Si oxide. In order to clarify a corrosion-resistant mechanism by Si addition and an effective range of temperature and oxygen concentration, short-term exposure tests, corrosion tests under low oxygen condition and transmission electron microscope observation of the thin

corrosion film will be necessary for Si-added steels.

As mentioned above, phenomena such as oxidation, dissolution, grain boundary corrosion, penetration of Pb-Bi and ferritization occurs during corrosion in static liquid Pb-Bi. Fig.25 summarizes the corrosion depth defined as the sum of thickness of corrosion film including internal oxidation layer, grain boundary corrosion depth and thickness of ferritization for several steels. The ratio of ferritization to the corrosion depth is large in 316ss and JPCA at 550℃. Table 2 also shows the total corrosion depth, thickness of corrosion film, grain boundary corrosion depth and thickness of ferritization for several steels after exposure to oxygen-saturated liquid Pb-Bi at 450 and 550℃ for 3000h.

The relationship between corrosion depth and Cr content in steels is shown in Fig.26. Corrosion depth of steels decreases at 450℃ with increasing Cr content of the steels regardless of ferritic/martensitic steels or austenitic steels. Corrosion depth of Si-added steel, SX, is very small. Corrosion depth of ferritic/martensitic steels which is shown as an open circle in Fig.26(b) also decreases at 550℃ with increasing Cr content of the steels while corrosion depth of austenitic steels, JPCA and 316ss becomes large because of formation of the ferrite layer at 550℃ in spite of their Cr content above 14%. Corrosion depth of SX containing 4.8%Si is very small at 550℃ in spite of austenitic steel since the protective film of Si oxide formed during exposure to Pb-Bi prevents dissolution of Ni and ferritization. In this way, it is considered that Si addition to steels is very effective for improvement of corrosion resistance in liquid Pb-Bi. However, Si is one of elements giving harmful influence on weldability and creep properties of steels. Furthermore, Si in steels may affect irradiation properties such as swelling, radiation induced segregation and embrittlement. It is necessary to evaluate the applicability of Si added steels to ADS components from the viewpoints of not only corrosion resistance in liquid Pb-Bi but also weldability and irradiation properties.

4. Conclusions

Static corrosion tests of various steels with different contents of Cr, Ni and Si were conducted in oxygen-saturated liquid Pb-Bi at 450℃ and 550℃ for 3000h. The following conclusions are drawn:

(1) Corrosion phenomena such as oxidation, grain boundary corrosion, dissolution of alloying elements and penetration of Pb and Bi occur in liquid Pb-Bi, where corrosion depth is defined as the sum of the thickness of the oxide film including internal oxidation, the grain boundary corrosion depth and the thickness of the formed ferrite layer.

(2) Corrosion depth at 450℃ decreases with increasing Cr content in steels regardless of ferritic/martensitic steels or austenitic steels. Appreciable dissolution of Ni and Cr does not occur in the three austenitic steels at 450℃. Thin oxide films are formed during exposure to liquid Pb-Bi up to 3000h.

(3) Corrosion depth of ferritic/martensitic steels at 550℃ decreases with increasing Cr content in steels. Nickel and chromium in austenitic steels, JPCA and 316ss dissolve into liquid Pb-Bi and the thick ferrite layer is formed at 550℃ in spite of formation of Fe-Cr oxide. As a result, corrosion depth of JPCA and 316ss become larger than that of ferritic/martensitic steels.

(4) A protective oxide film composed of Si and O is formed on the surface of SX containing 4.8%Si during corrosion in liquid Pb-Bi at 550℃. The thin oxide film prevents dissolution of Ni and Cr into Pb-Bi. The Si added austenitic steel exhibits good corrosion resistance at 550℃ up to 3000h and under static condition in liquid Pb-Bi.

References

[1] T.A. Gabriel, J.R. Haines, T.J. McManamy, J. Nucl. Mater., 318(2003)1.

[2] The joint project team of JAERI and KEK, JAERI-Tech 99-56, 1999.

[3] C. Rubbia, J.A. Rubio, S. Buono, F. Carminati, Conceptual design of a fast neutron operated high power energy amplifier, CERN/AT/95-44(ET), September 29, 1995.

[4] T. Mukaiyama, T. Takizuka, M. Mizumoto, Y. Ikeda, T. Ogawa, A. Hasegawa, H. Takada and H. Takano, Progress in Nuclear Energy, 38 (2001)107.

[5] B. F. Gromov, Y. I. Orlov, P. N. Martynov and V. A. Gulevsky, Proceedings of Heavyy Liquid Metal Coolants in Nuclear Technology, HLMC'98, October 5-9, 1998, Obninsk, Russia, (1999) p.87.

[6]J .R.Weeks Nucl. Eng. Design 15(1971)363.

[7] I. V. Gorynin, G. P. Karzov, V. G. Markov, V. S. Lavrukihin and V. A. Yakovlev, Proceedings of Heavy Liquid Metal Coolants in Nuclear Technology, HLMC'98, October 5-9, 1998, Obninsk, Russia, (1999) p.120.

[8] G.S. Yachmenyov, A.Ye. Rusanov, B. F. Gromov, Yu. S. Belomytsev, N. S. Skvortsov, A. P. Demishonkov, Proceedings of Heavy Liquid Metal Coolants in Nuclear Technology, HLMC'98, October 5-9, 1998, Obninsk, Russia, (1999) p.133.

[9] F.Barbier, A. Rusanov, J. Nucl. Mater., 296(2001)231.

[10]C. Fazio, G. Benamati, C. Martini, G. Palombarini, J. Nucl. Mater., 296(2001)243.

[11]G. Benamti, C. Fazio, H. Piankova, A. Rusanov, J. Nucl. Mater., 301(2002)23.

[12] Y. Kurata, M. Futakawa, K. Kikuchi, S. Saito, T. Osugi, J. Nucl. Mater., 301(2002)28.

[13] K.Kikuchi, Y.Kurata, S.Saito, M.Futakawa, T.Sasa, H.Oigawa, E.Wakai, K.Miura, J. Nucl. Mater., 318(2003)348.

[14] G.Mueller, G. Schumacher, F. Zimmermann, J. Nucl. Mater., 278(2000)85.

[15] F.Barbier, G. Benamati, C. Fazio, A. Rusanov, J. Nucl. Mater., 295(2001)149.

[16] G.Mueller, A.Heinzel, J.Konys, G. Schumacher, A.Weisenburger, F.Zimmermann, V.Engeliko, A.Rusanov, V.Markov, J. Nucl. Mater., 301(2002)40.

[17] G.Mueller, A.Heinzel, J.Konys, G. Schumacher, A.Weisenburger, F.Zimmermann, V.Engeliko, A.Rusanov, V.Markov, J. Nucl. Mater., 335(2004)163.

[18] A. Aiello, M. Azzati, G. Benamati, A. Gessi, B. Long, G. Scaddozzo, J. Nucl. Mater., 335(2004)169.

[19] D. Gomez-Briceno, L. Soler, F. J. Martin, F. Hernandez, J. Nucl. Mater., 303(2002)137.

[20] L. Soler, F. J. Martin, F. Hernandez, D. Gomez-Briceno, J. Nucl. Mater., 335(2004)174.

[21] Ph. Deloffre, F. Balbaud-Celerier, A. Terlain, J. Nucl. Mater., 335(2004)180.
[22] F. Gnecco, E. Ricci, C. Bottino, A. Passerone, J. Nucl. Mater., 335(2004)185.
[23] T. Furukawa, G.Mueller, G. Schumacher, A.Weisenburger, A.Heinzel, F. Zimmermann, K. Aoto, J. Nucl. Sci. Technol., 41(2004)265.
[24] T. Furukawa, G.Mueller, G. Schumacher, A.Weisenburger, A.Heinzel, F. Zimmermann, K. Aoto, J. Nucl. Mater., 335(2004)189.
[25] F. J. Martin, L. Soler, F. Hernandez, D. Gomez-Briceno, J. Nucl. Mater., 335(2004)194.
[26] F. Balbaud-Celerier, A. Terlain, J. Nucl. Mater., 335(2004)204.
[27] G. Ilincev, D. Karnik, M. Paulobic, A. Doubkova, J. Nucl. Mater., 335(2004)210.
[28] Y. Kurata, M. Futakawa, J. Nucl. Mater., 325(2004)217.
[29] J.Robertson, M. I. Manning, Mater. Sci. Technol., 5 (1989)741.

Table 1 Chemical composition of materials tested in the static corrosion experiment (mass%)

	C	Si	Mn	Cr	Ni	Mo	Fe	V	N	W	Ti	Al	Cu
F82H	0.095	0.10	0.01	7.72	<0.02	<0.01	balance	0.18	0.010	1.95	0.005	<0.001	-
Mod.9Cr-1Mo steel	0.10	0.30	0.40	8.41	0.06	0.88	balance	0.20	0.047	<0.0005	<0.01	0.033	-
14Cr-16Ni-2Mo(JPCA)	0.058	0.50	1.54	14.14	15.87	2.29	balance	0.03	0.003	0.010	0.22	0.012	-
410ss	0.067	0.31	0.80	12.21	0.12	0.02	balance	0.07	0.013	-	<0.01	0.002	-
430ss	0.080	0.52	0.23	16.24	0.15	0.02	balance	0.10	0.024	-	<0.01	0.007	-
2.25Cr-1Mo steel	0.10	0.34	0.44	2.18	0.02	0.92	balance	0.01	0.009	-	<0.01	0.002	-
Fe	0.002	-	-	-	-	-	balance	-	0.001	-	-	-	-
316ss	0.04	0.69	1.22	16.83	10.79	2.06	balance	-	-	-	-	-	-
SX	0.010	4.80	0.60	17.58	19.08	0.356	balance	-	-	-	-	-	2.14

Table 2 Corrosion depth of several steels in oxygen-saturated Pb-Bi at 450℃ and 500℃ for 3000h (μm)

	Material	Corrosion film	Grain boundary corrosion	Ferritization	Total corrosion depth
450℃	F82H	4.93	3.46		8.39
	Mod.9Cr-1Mo	6.06	2.35		8.41
	JPCA	2.76			2.76
	410ss	2.83			2.83
	2.25Cr-1Mo	11.52	1.15		12.67
	316ss	2.58			2.58
	SX	0.3			0.3
550℃	F82H	13.95(6.19)			13.95
	Mod.9Cr-1Mo	13.97(7.32)			13.97
	JPCA	2.88		43.6	46.48
	410ss	2.58	2.84		5.42
	2.25Cr-1Mo	11.09	12.93		24.02
	316ss	2.96		22.41	25.37
	SX	0.48			0.48

( ):Internal oxidation

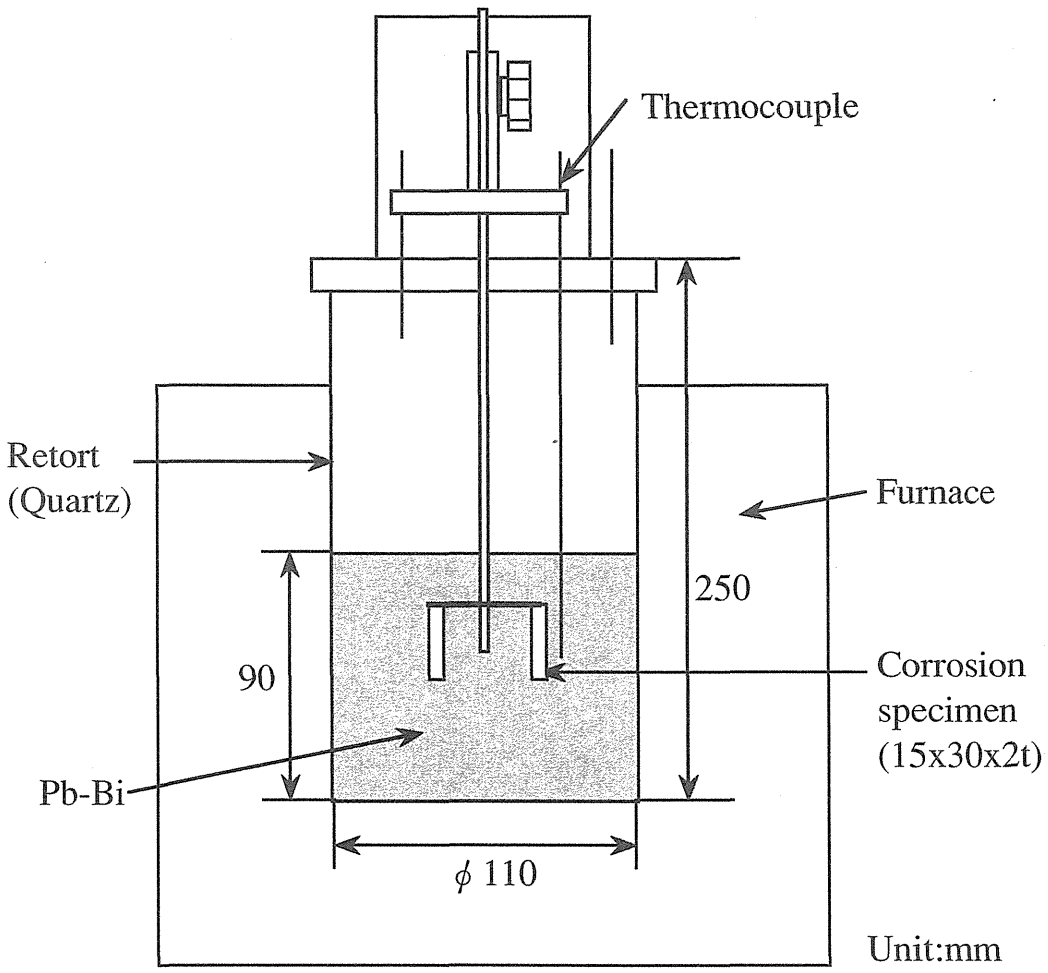

Fig. 1 Schematic diagram of corrosion test apparatus in liquid Pb-Bi

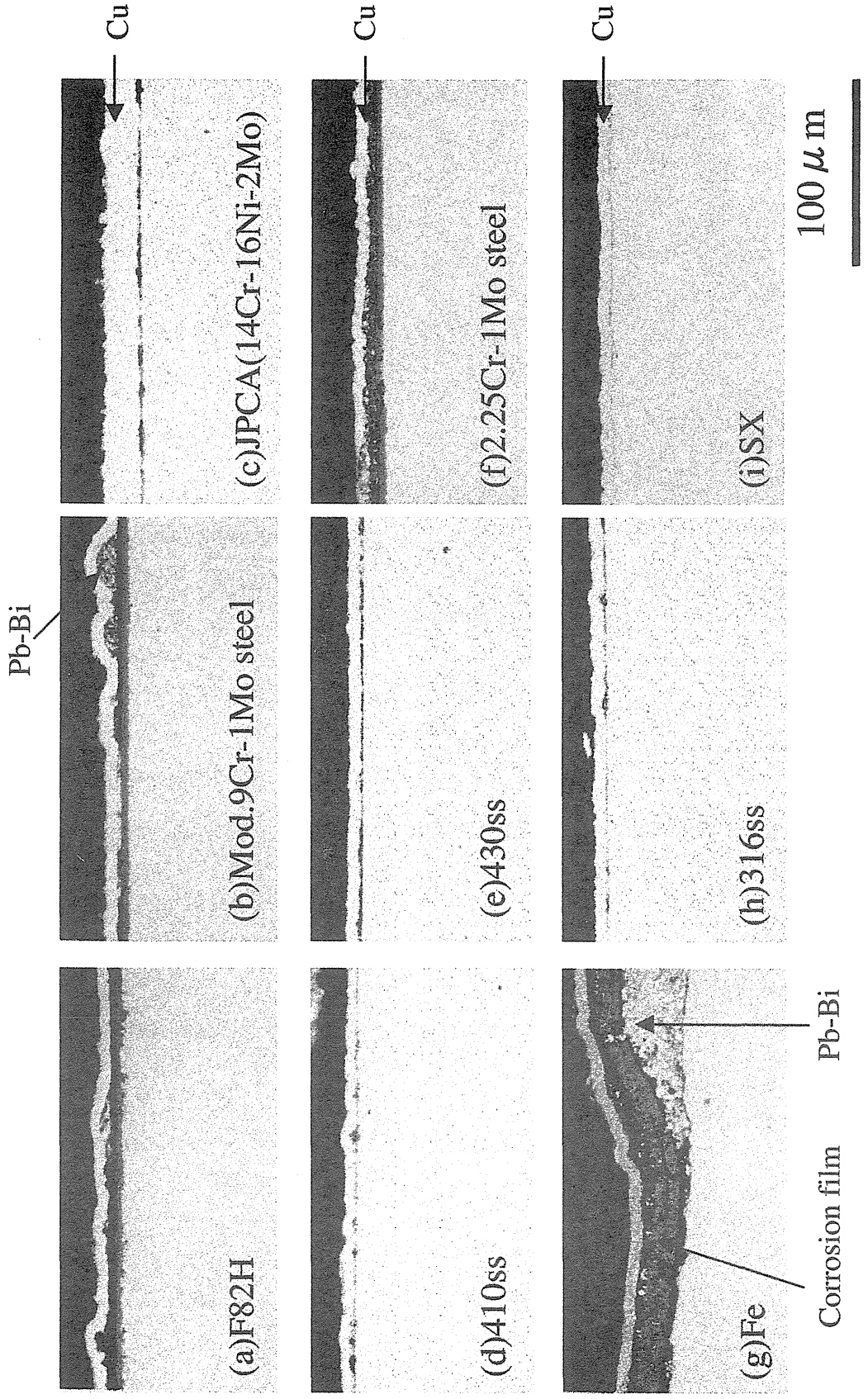

Fig.2 Optical micrographs of cross sections of (a) F82H, (b) Mod.9Cr-1Mo steel, (c) JPCA, (d)410ss, (e)430ss, (f)2.25Cr-1Mo steel, (g)Fe, (h)316ss and (i)SX after corrosion in liquid Pb-Bi at 450℃.

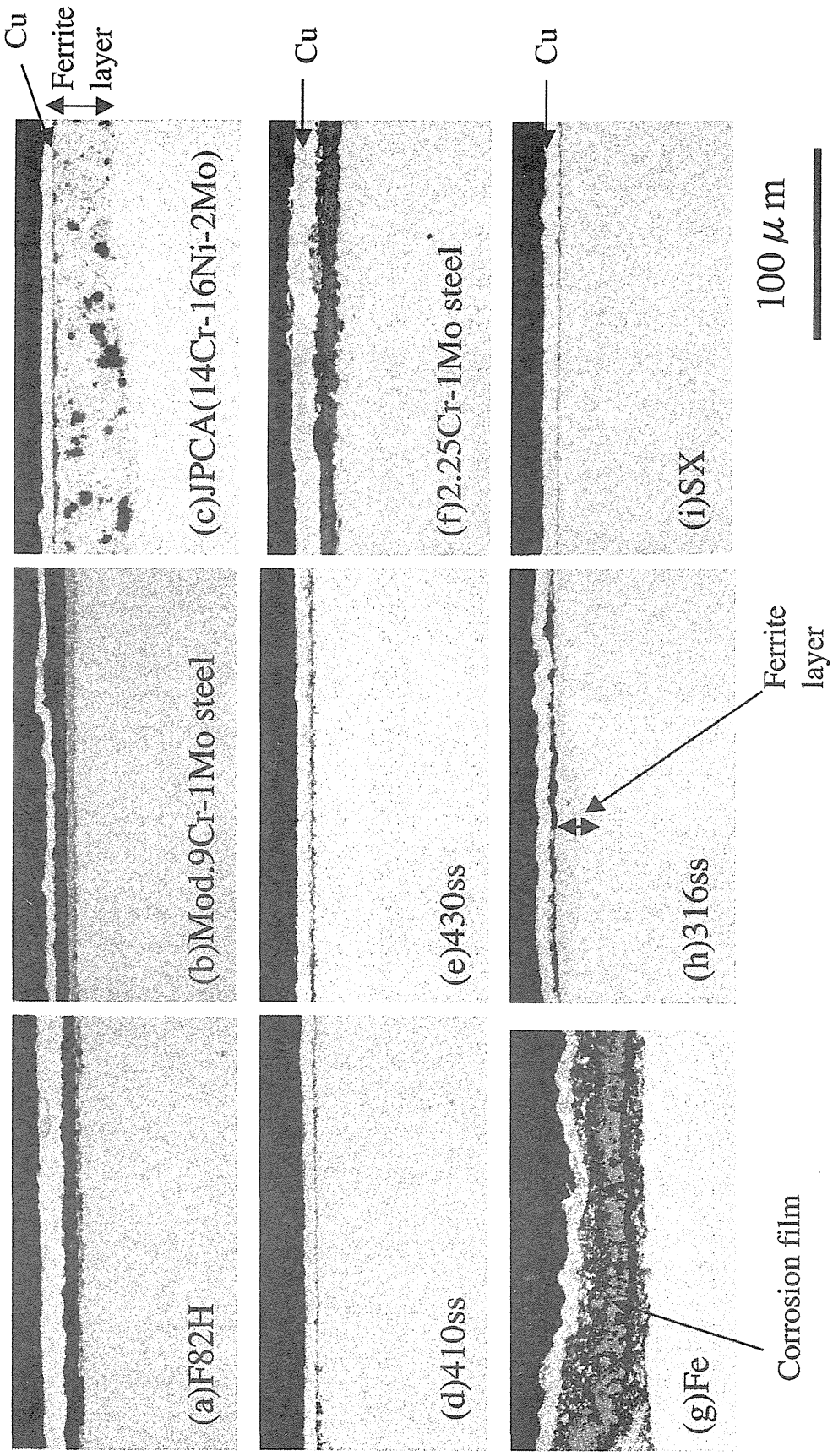

Fig.3 Optical micrographs of cross sections of (a) F82H, (b) Mod.9Cr-1Mo steel, (c) JPCA, (d)410ss, (e)430ss, (f)2.25Cr-1Mo steel, (g)Fe, (h)316ss and (i)SX after corrosion in liquid Pb-Bi at 550℃.

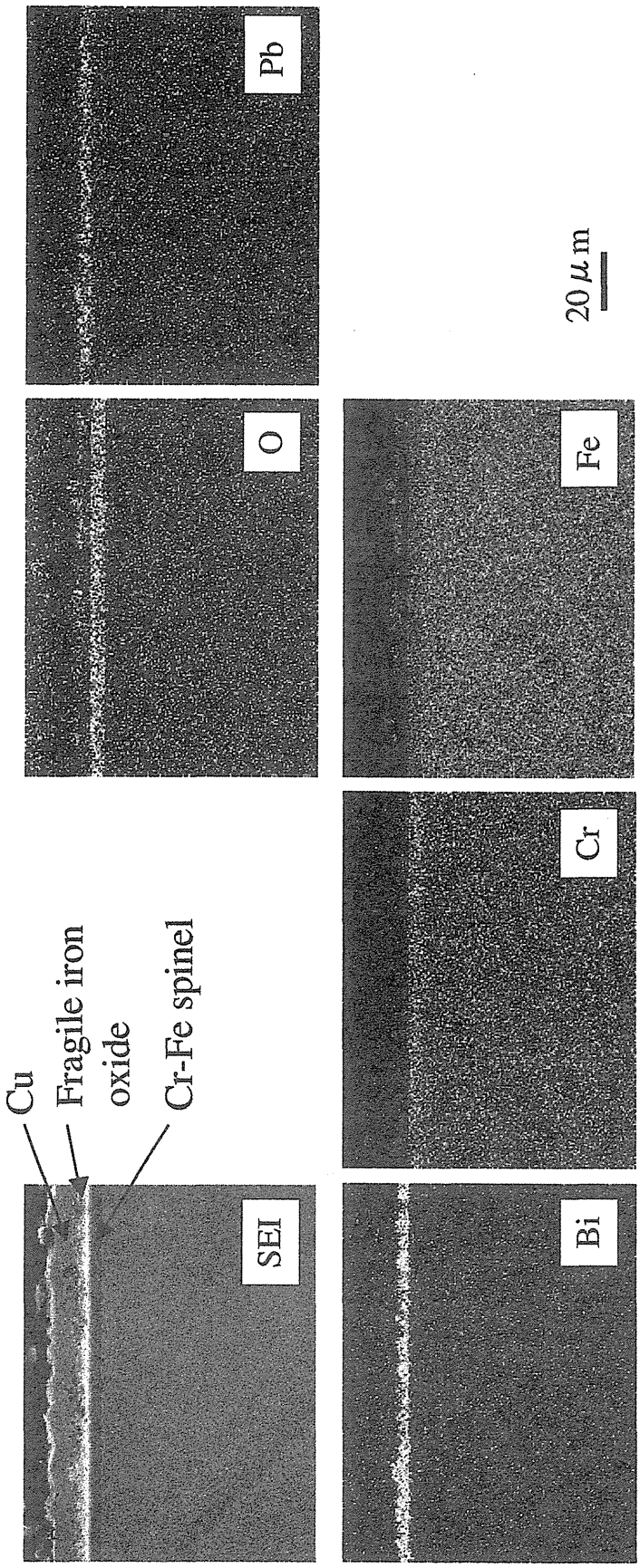

Fig.4 EDX analysis of the cross section of Mod.9Cr-1Mo steel after corrosion in liquid Pb-Bi at 450°C for 3000h.

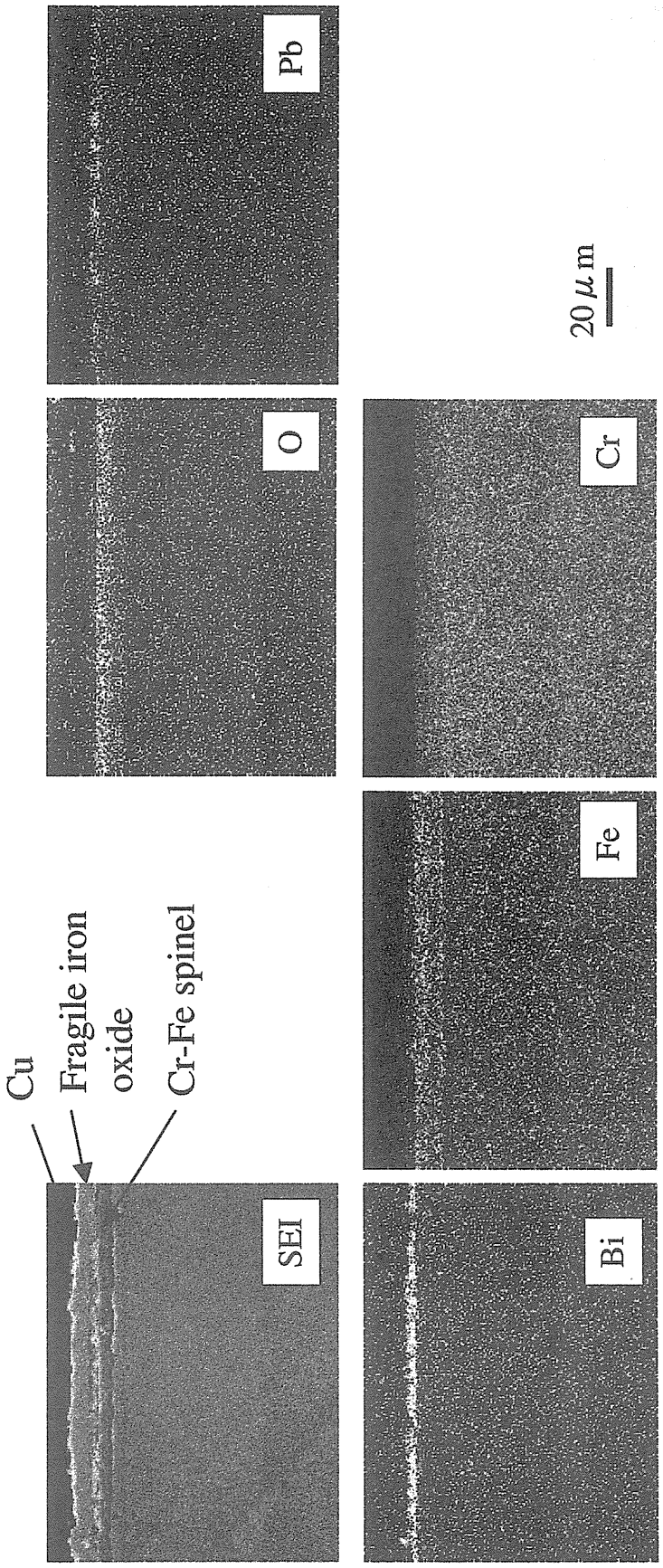

Fig.5 EDX analysis of the cross section of Mod.9Cr-1Mo steel after corrosion in liquid Pb-Bi at 550°C for 3000h.

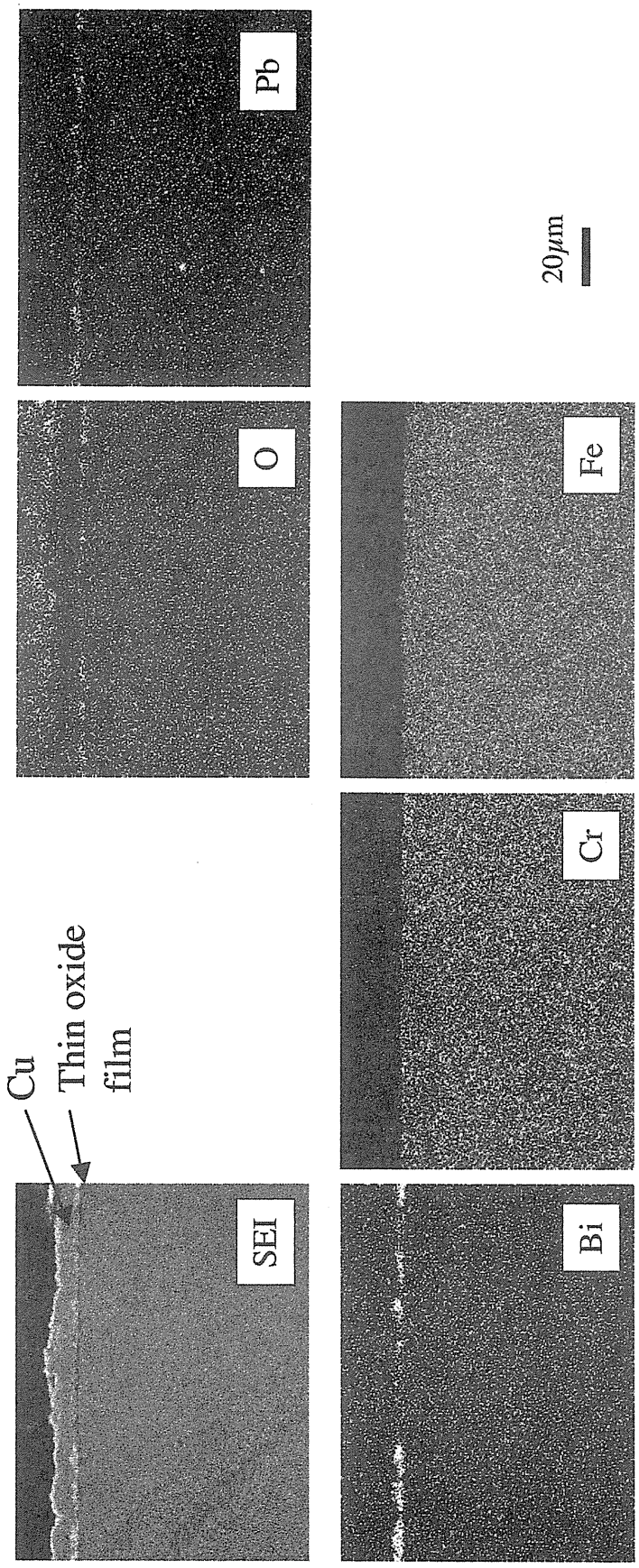

Fig.6 EDX analysis of the cross section of type 410ss after corrosion in liquid Pb-Bi at 450°C for 3000h.

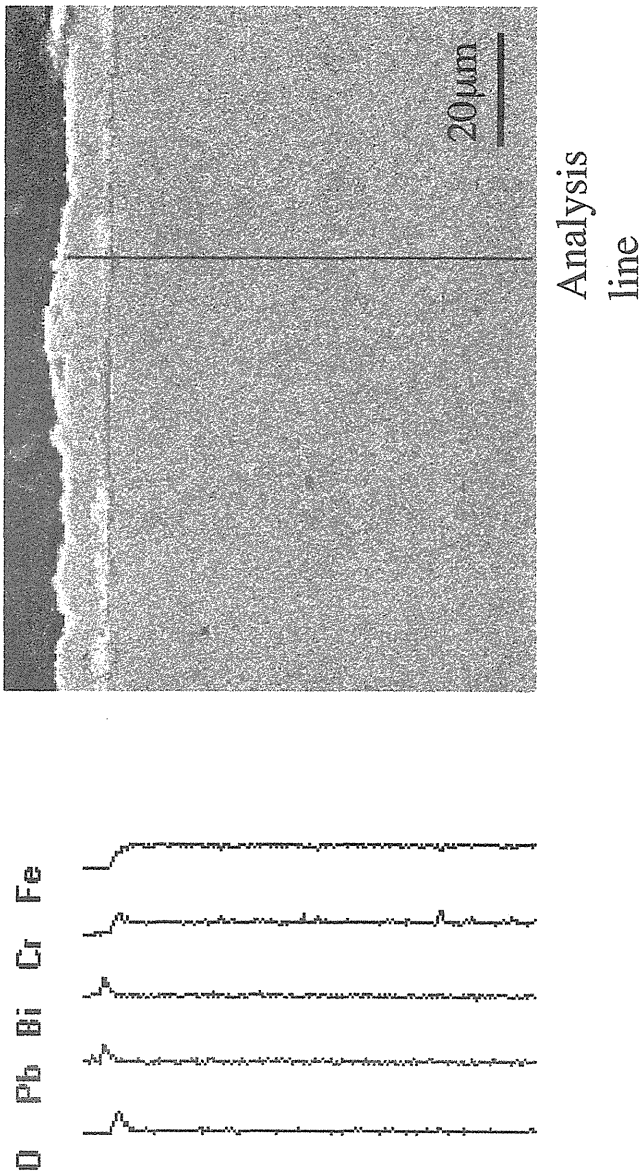

Fig.7 Line analysis of the cross section of type 410ss after corrosion in liquid Pb-Bi at 450°C for 3000h.

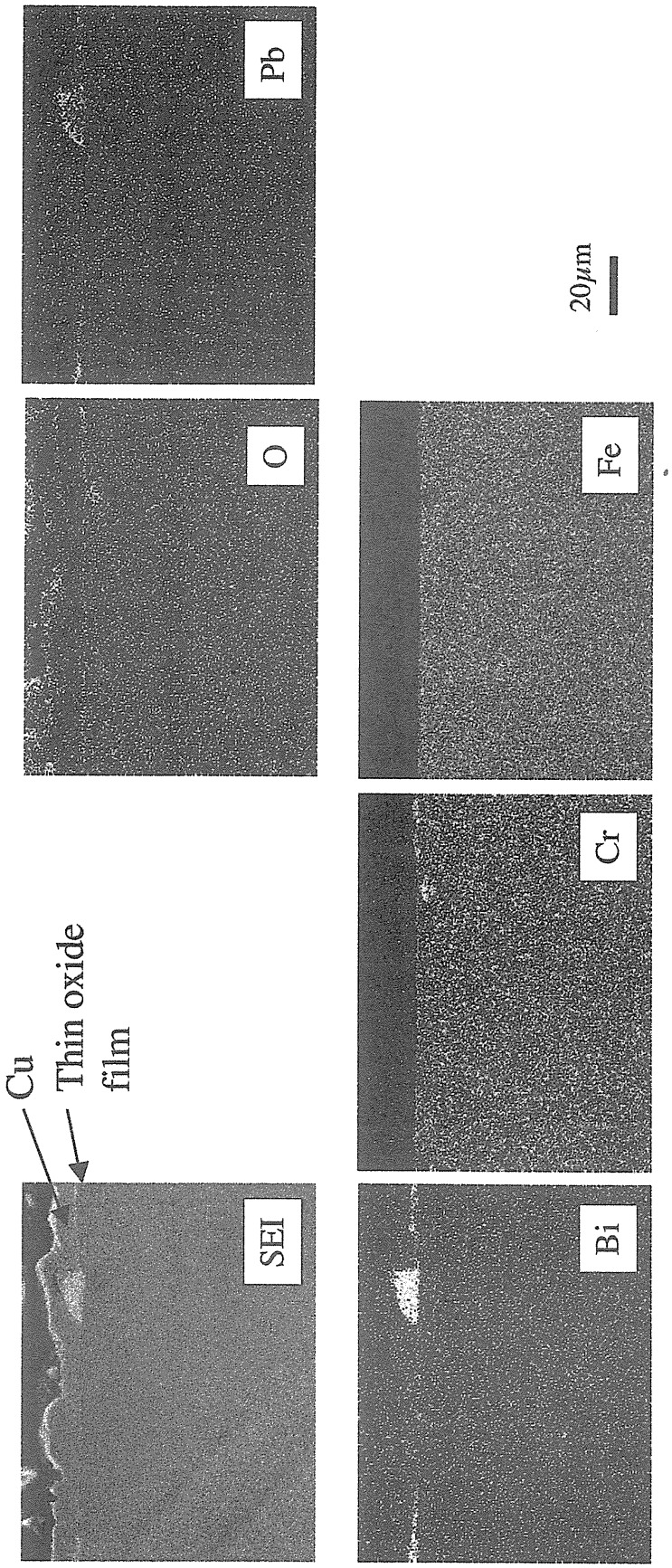

Fig.8 EDX analysis of the cross section of type 410ss after corrosion in liquid Pb-Bi at 550°C for 3000h.

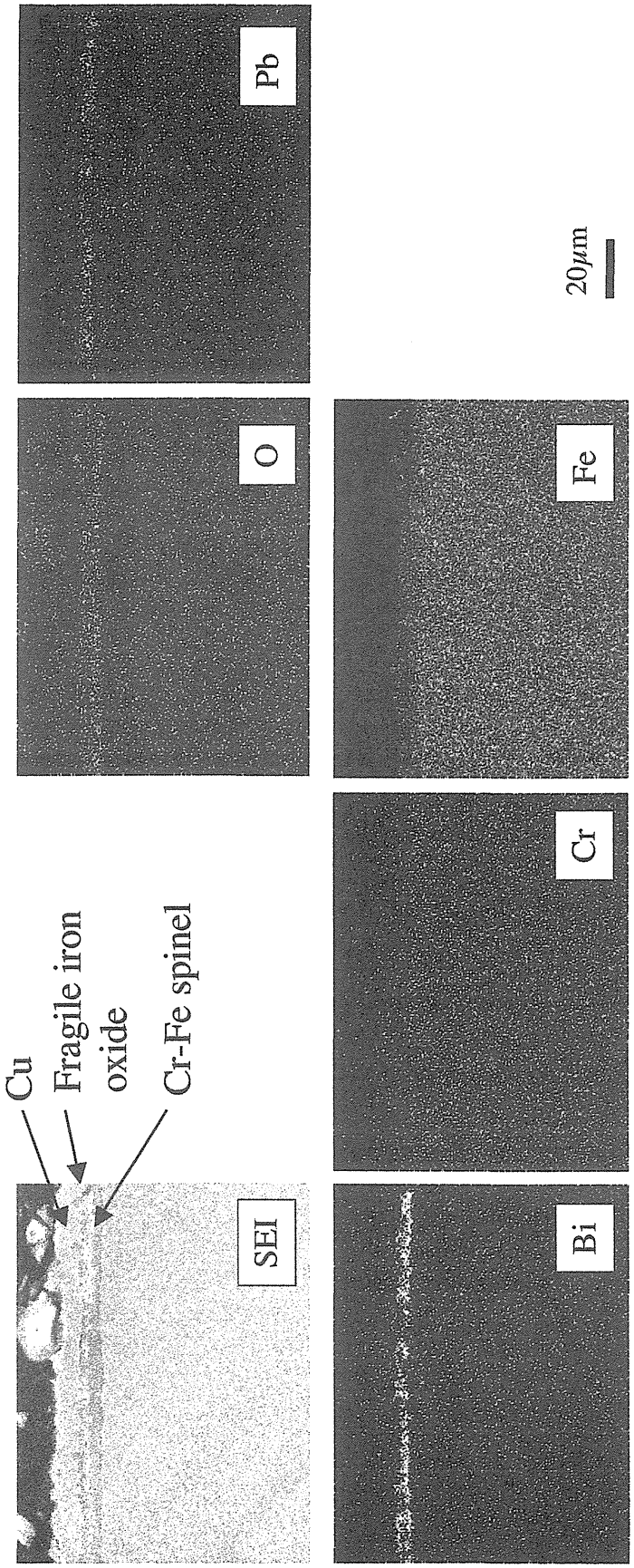

Fig.9 EDX analysis of the cross section of 2.25Cr-1Mo steel after corrosion in liquid Pb-Bi at 450°C for 3000h.

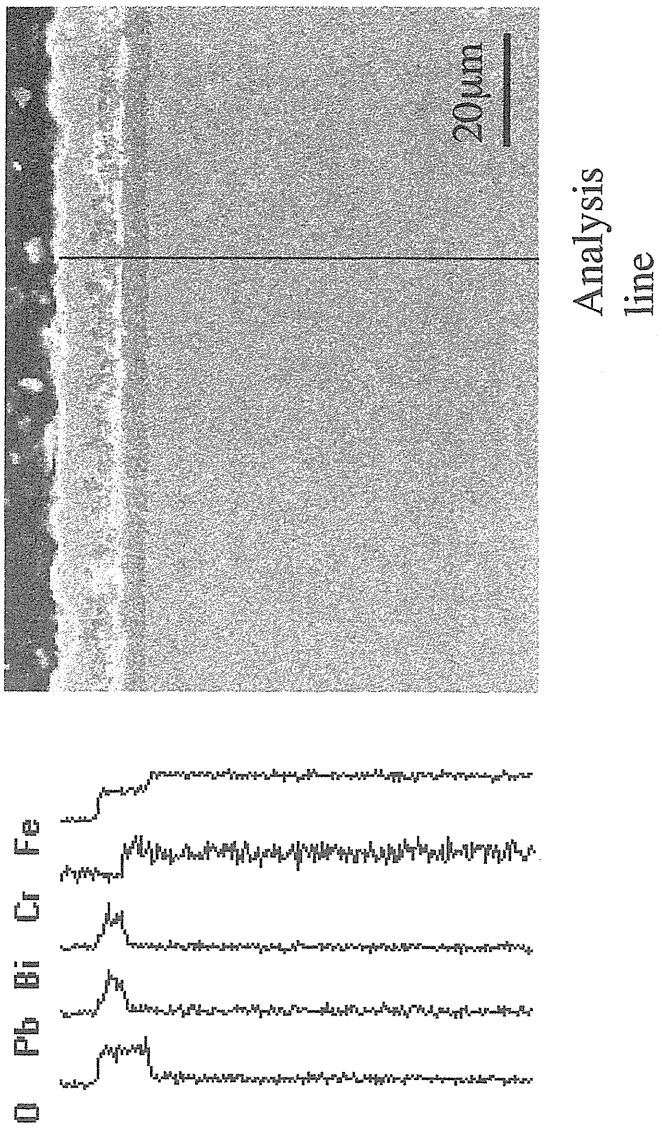

Fig.10 Line analysis of the cross section of 2.25Cr-1Mo steel after corrosion in liquid Pb-Bi at 450°C for 3000h.

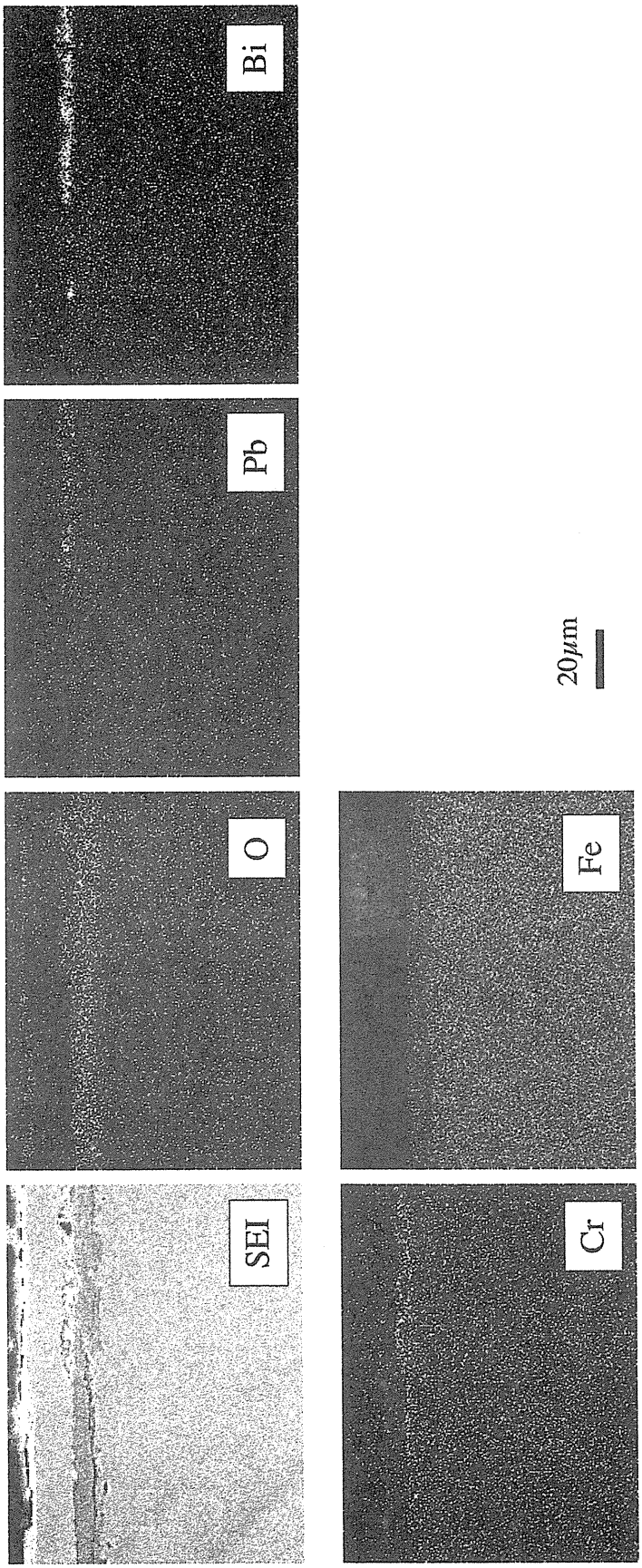

Fig.11 EDX analysis of the cross section of 2.25Cr-1Mo steel after corrosion in liquid Pb-Bi at 550°C for 3000h.

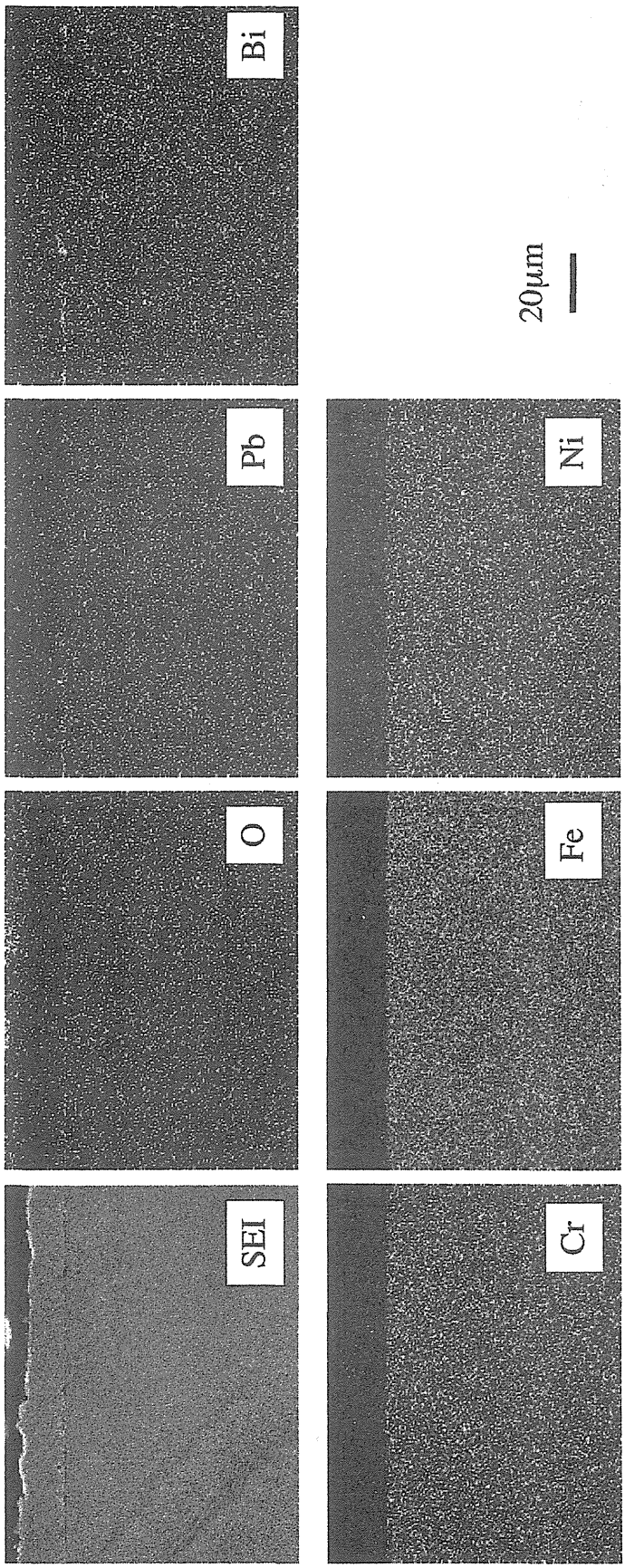

Fig.12 EDX analysis of the cross section of JPCA specimen after corrosion in liquid Pb-Bi at 450°C for 3000h.

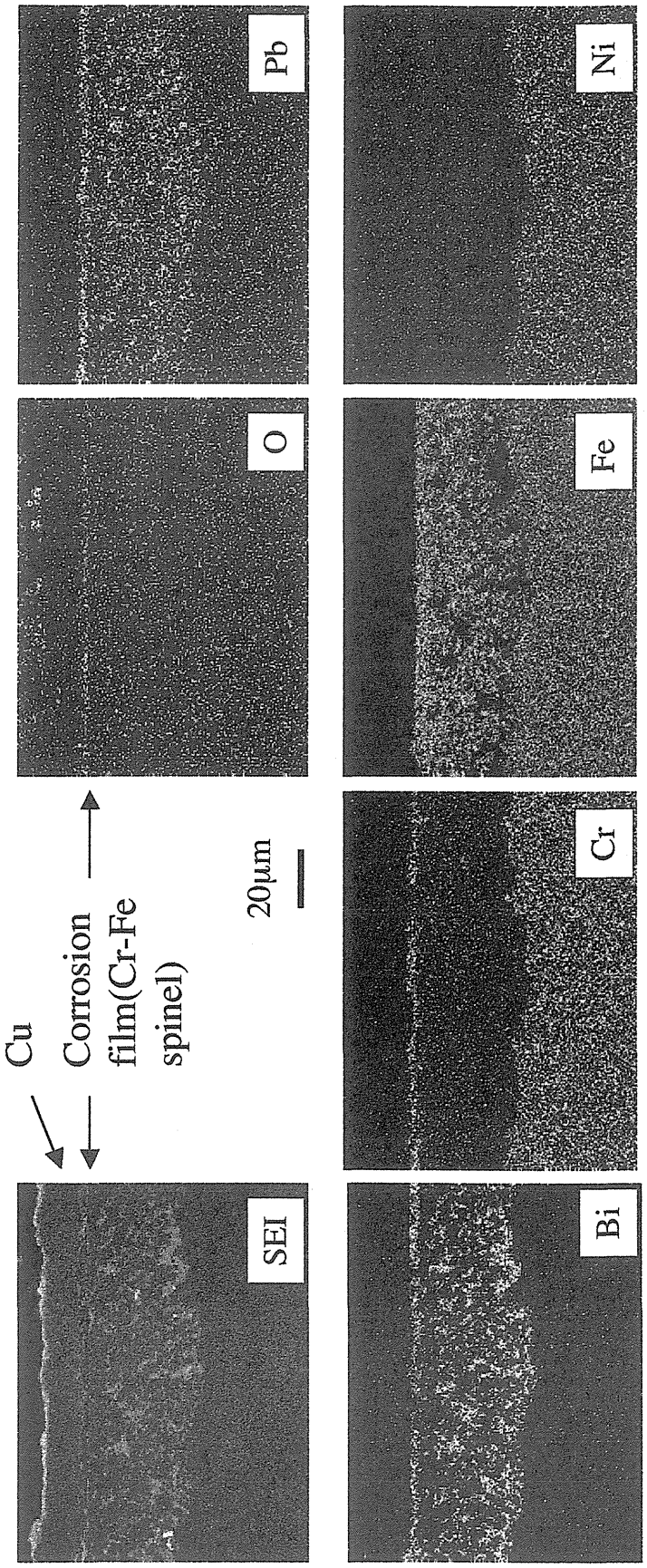

Fig.13 EDX analysis of the cross section of JPCA after corrosion in liquid Pb-Bi at 550°C for 3000h.

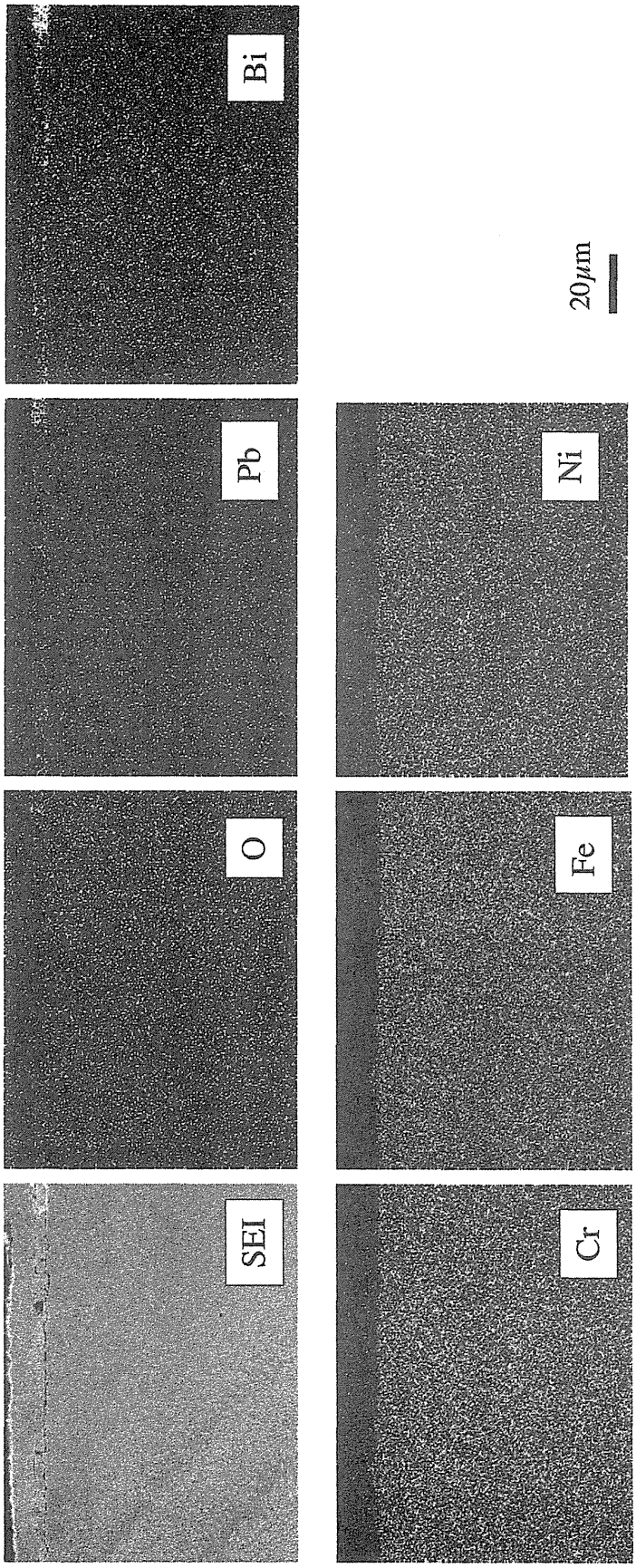

Fig.14 EDX analysis of the cross section of type 316ss after corrosion in liquid Pb-Bi at 450°C for 3000h.

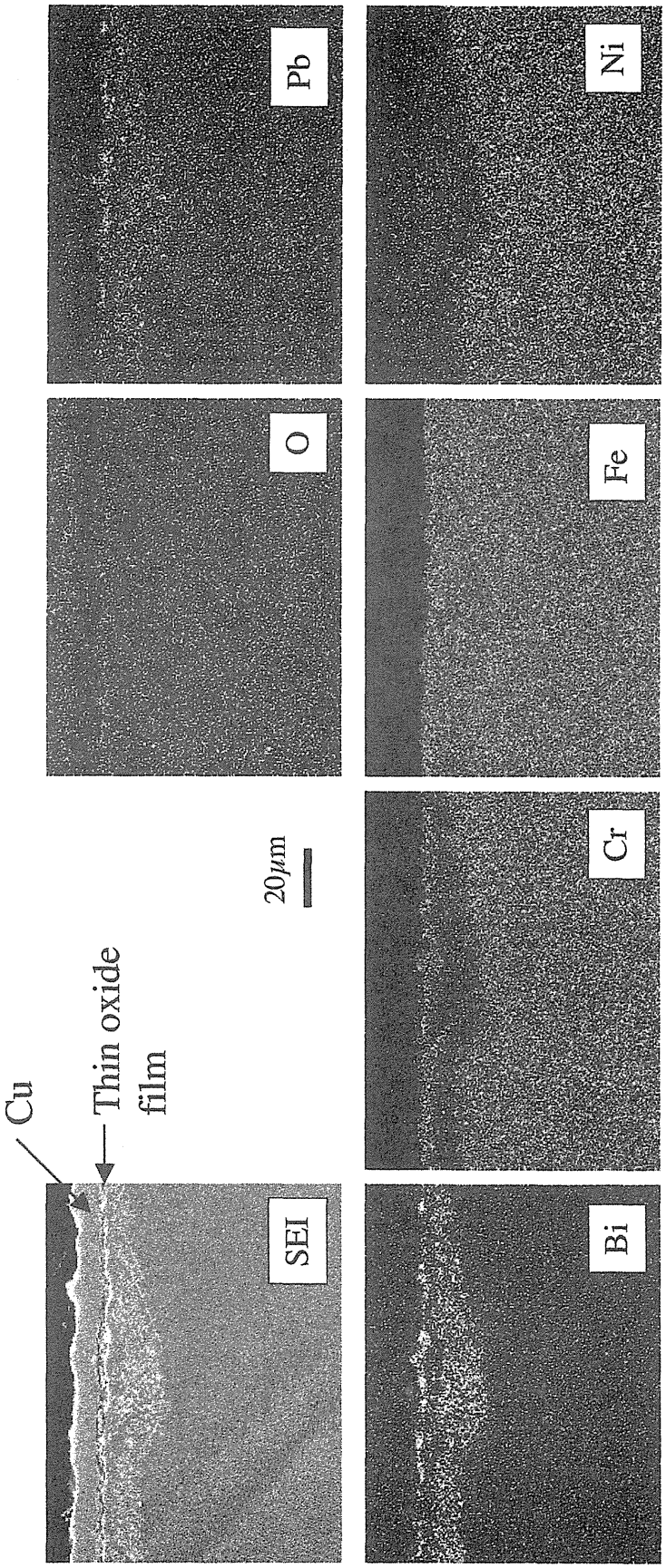

Fig.15 EDX analysis of the cross section of type 316ss after corrosion in liquid Pb-Bi at 550°C for 3000h.

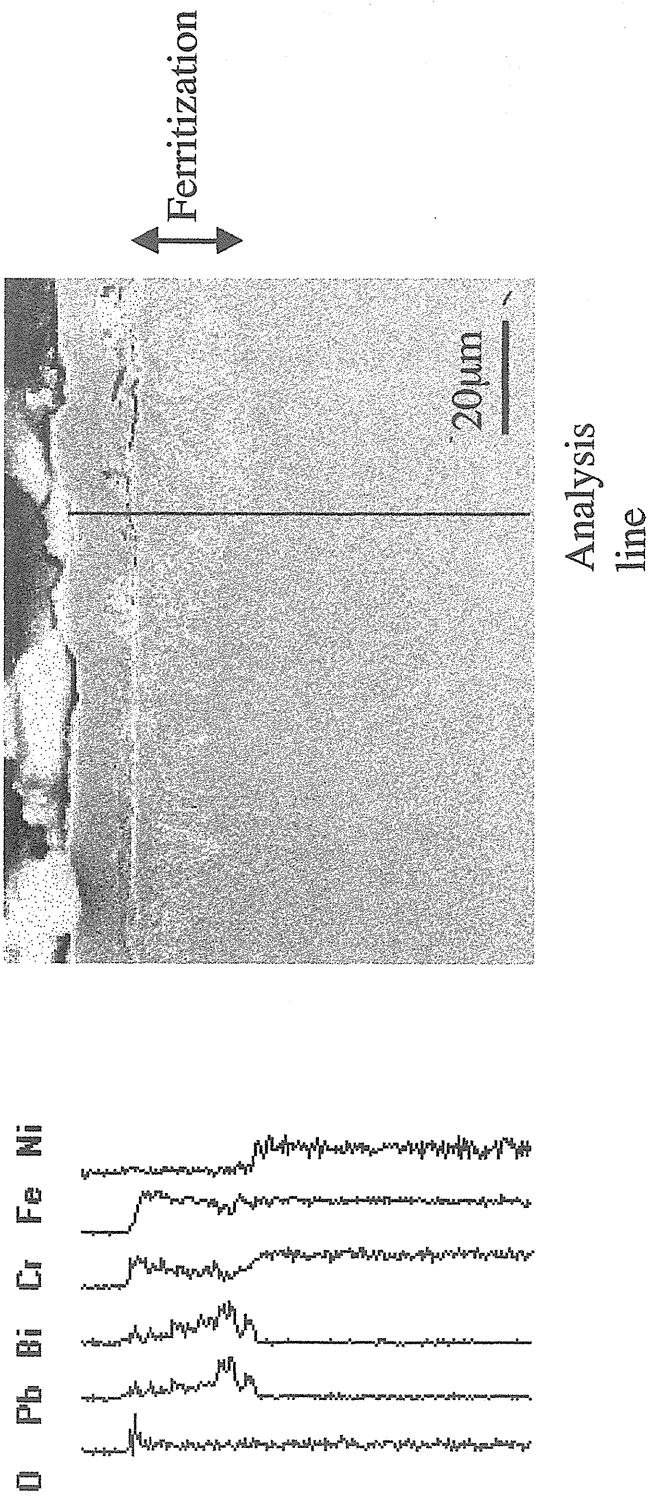

Fig.16 Line analysis of the cross section of type 316ss after corrosion in liquid Pb-Bi at 550°C for 3000h.

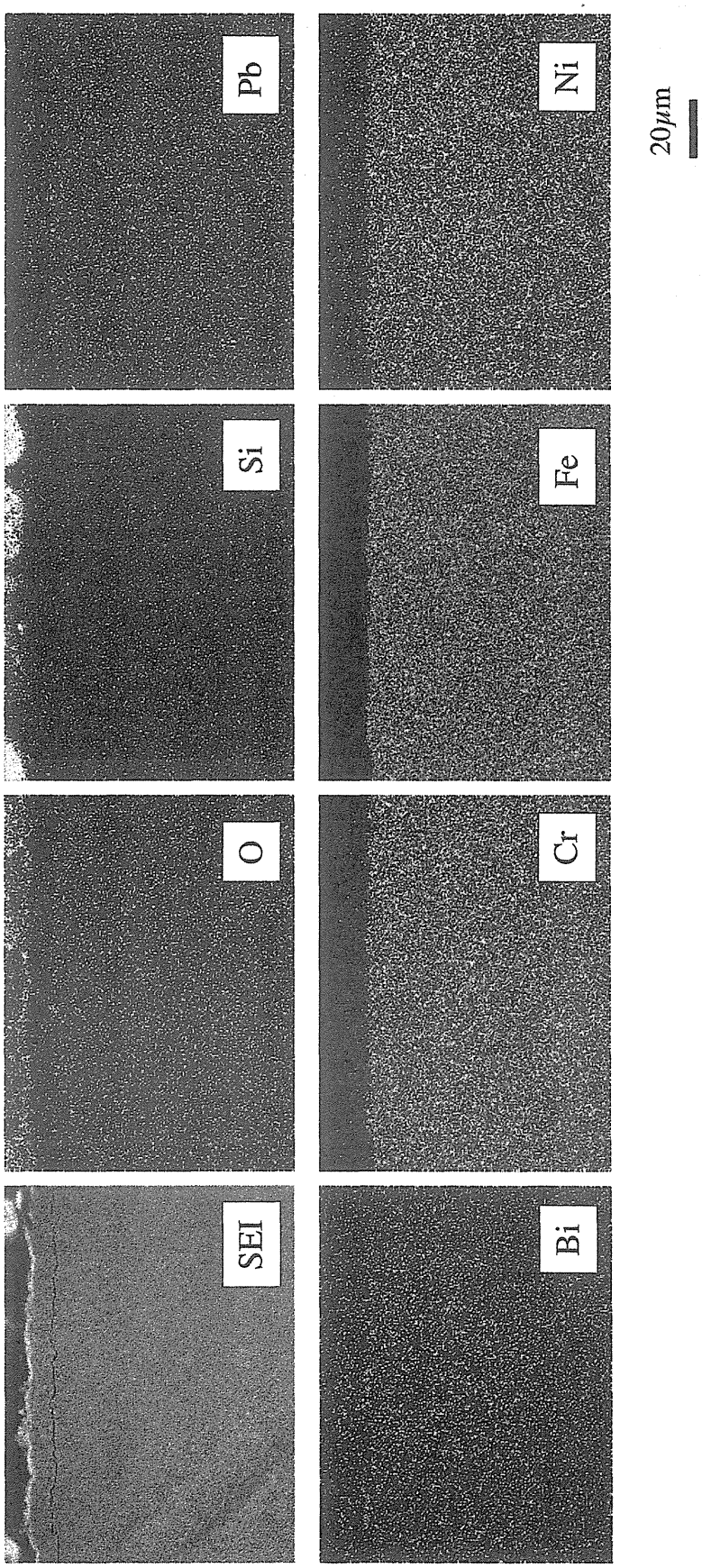

Fig.17 EDX analysis of the cross section of SX after corrosion in liquid Pb-Bi at 450°C for 3000h.

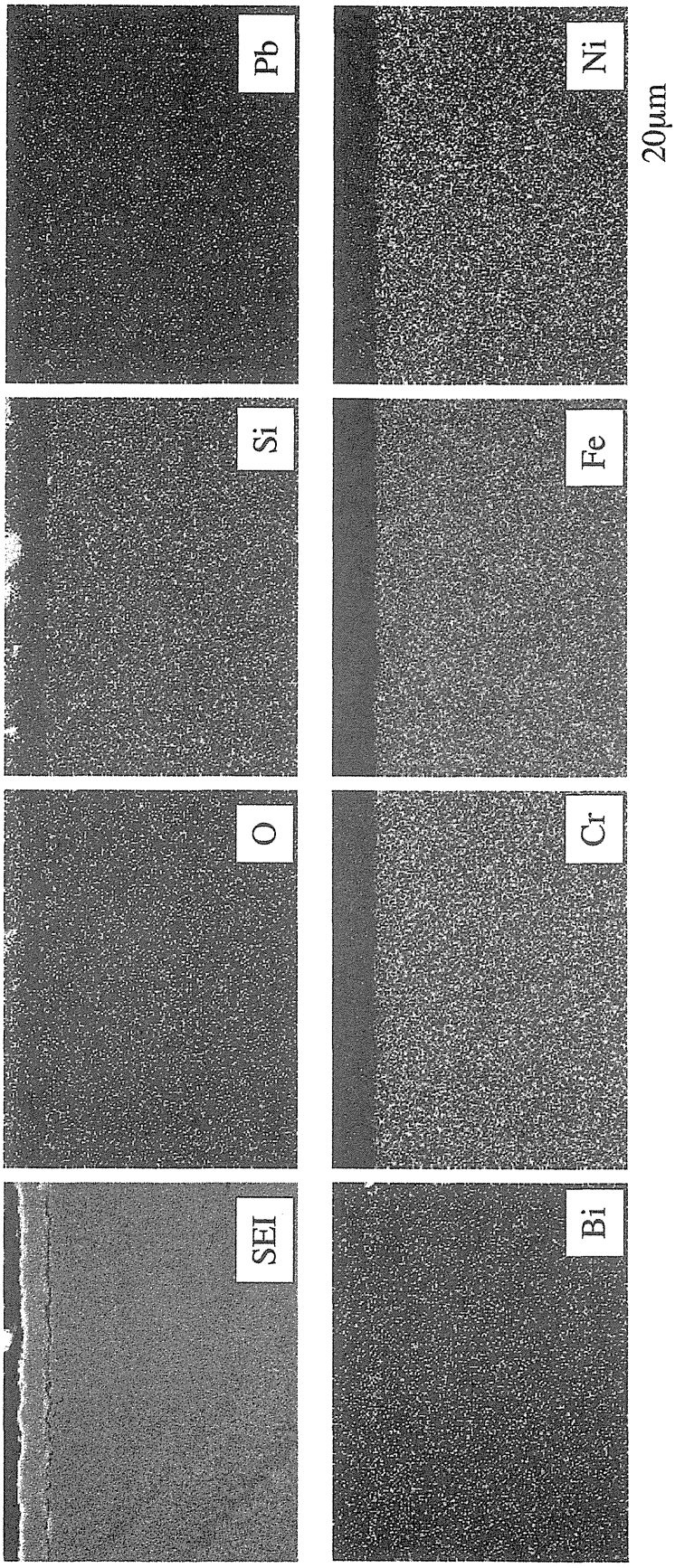

Fig.18 EDX analysis of the cross section of SX after corrosion in liquid Pb-Bi at 550°C for 3000h.

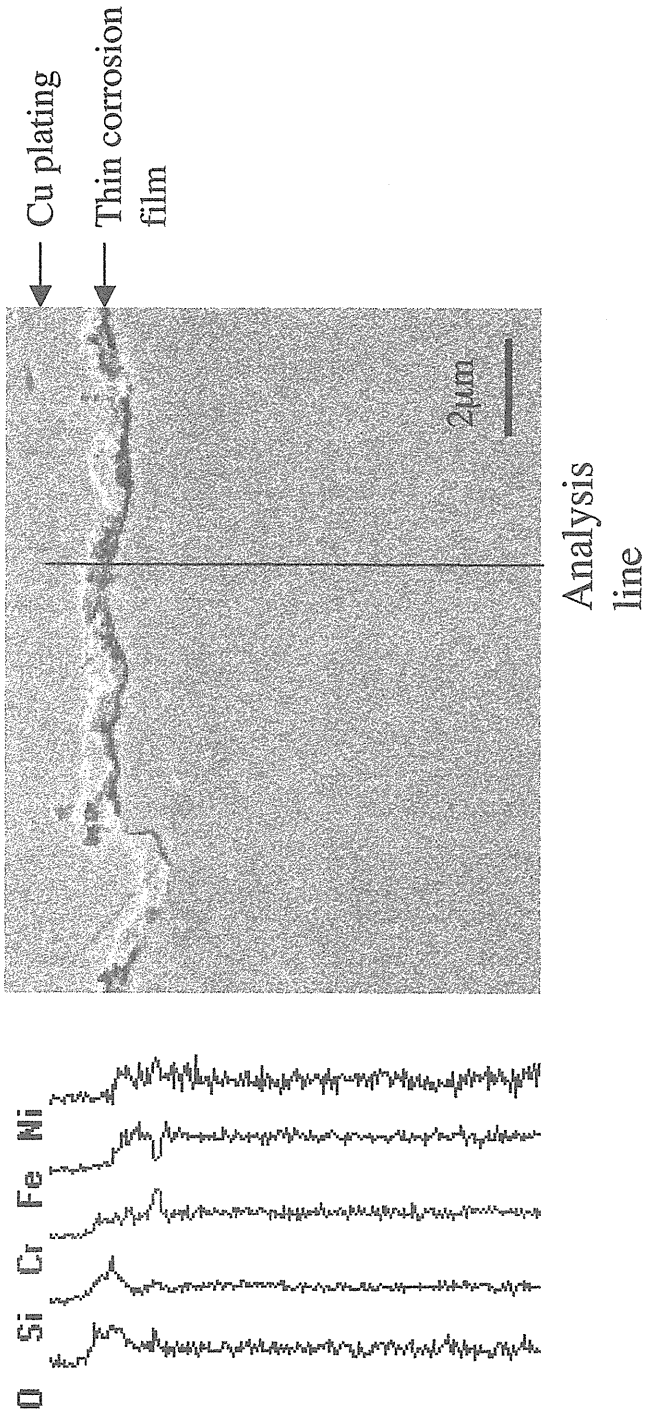

Fig.19 Line analysis of the cross section of SX after corrosion in liquid Pb-Bi at 550°C for 3000h.

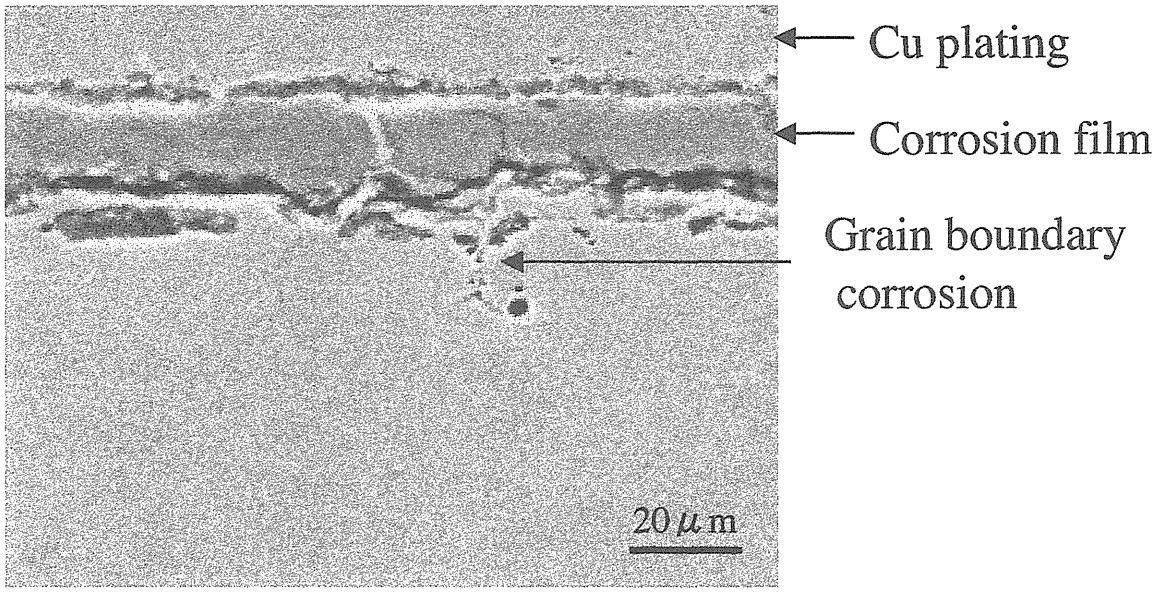

Fig.20 SEM image of cross section of 2.25Cr-1Mo steel after corrosion in liquid Pb-Bi at 550°C for 3000h.

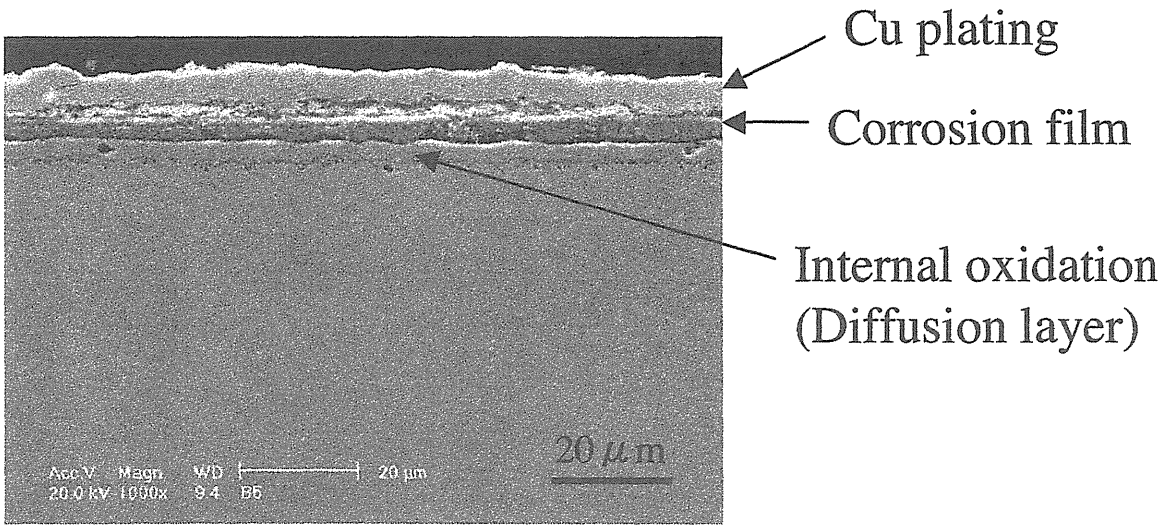

Fig.21 SEM image of cross section of Mod.9Cr-1Mo steel after corrosion in liquid Pb-Bi at 550°C for 3000h.

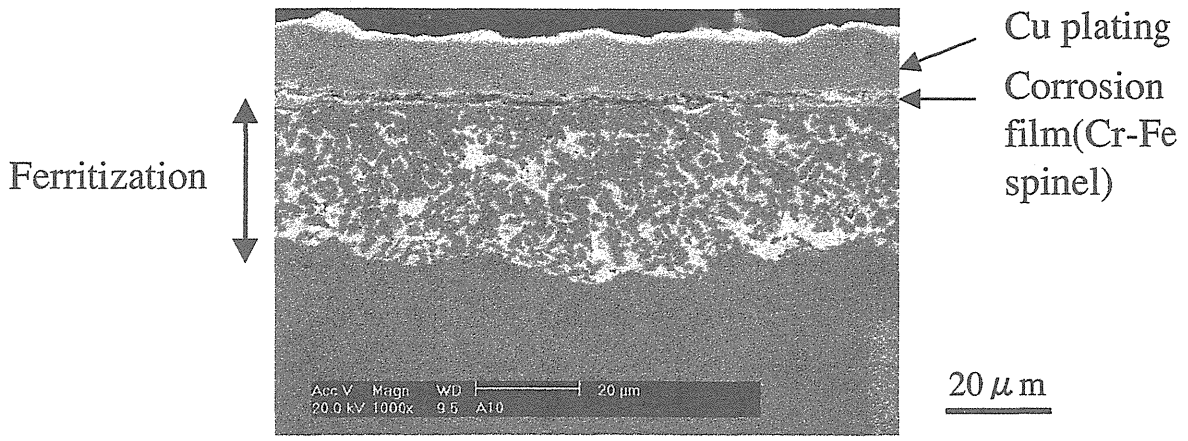

Fig.22 SEM image of cross section of JPCA after corrosion in liquid Pb-Bi at 550°C for 3000h.

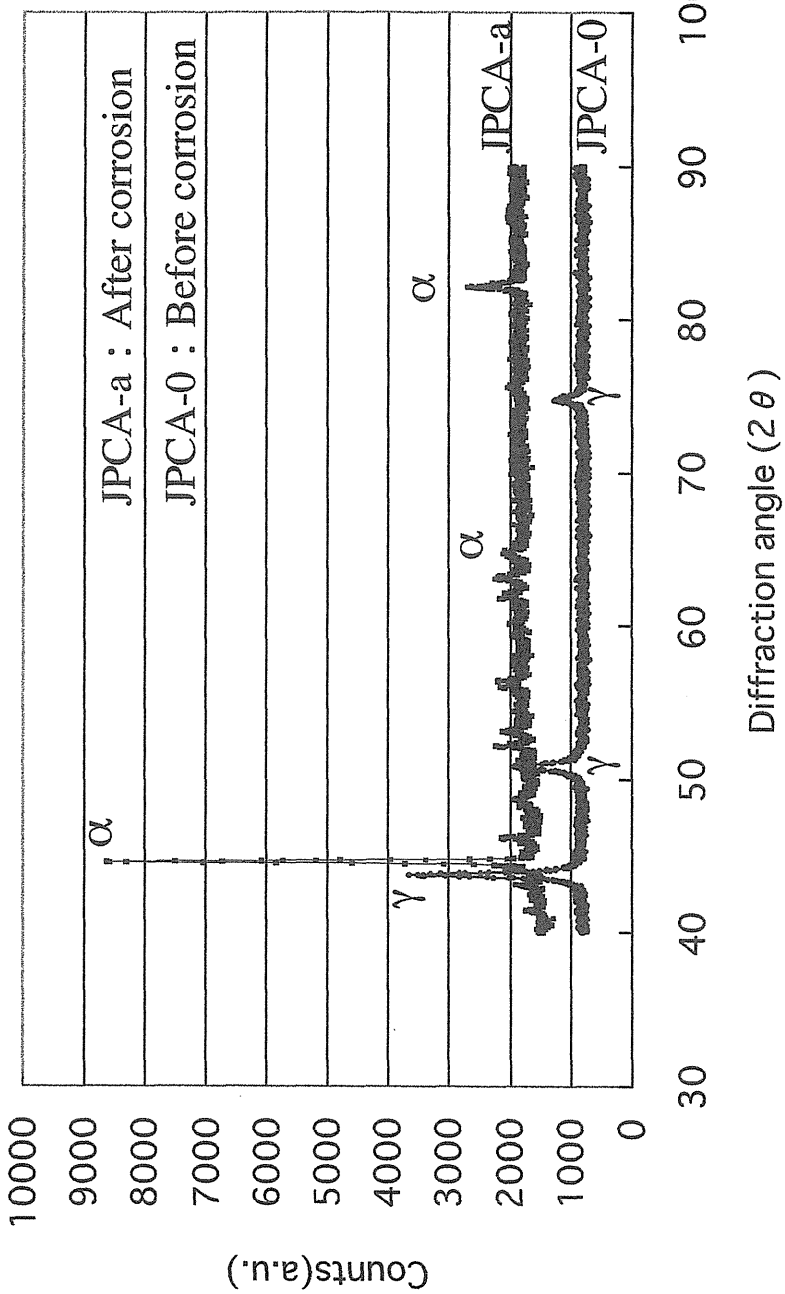

Fig.23 X-ray diffraction spectra of JPCA before and after corrosion at 550℃.

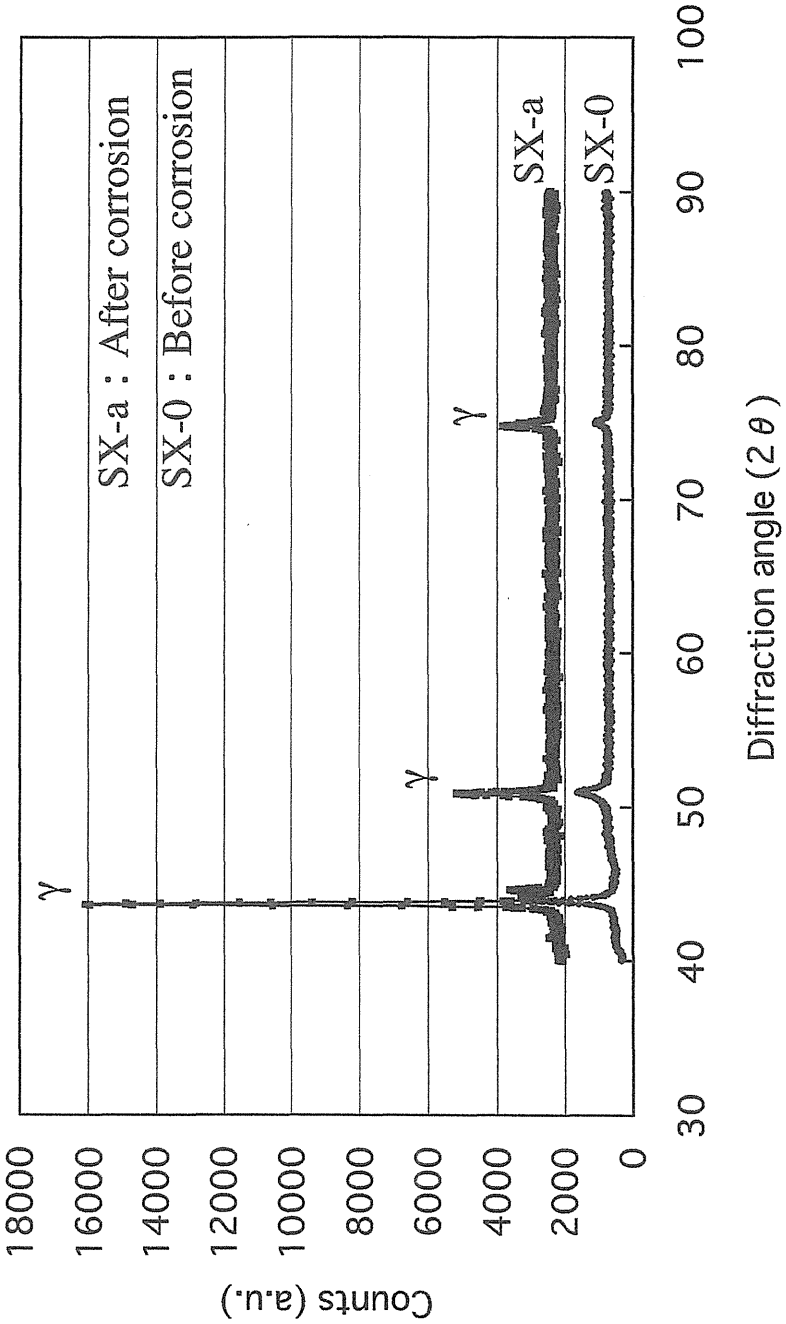

Fig.24 X-ray diffraction spectra of SX before and after corrosion at 550℃.

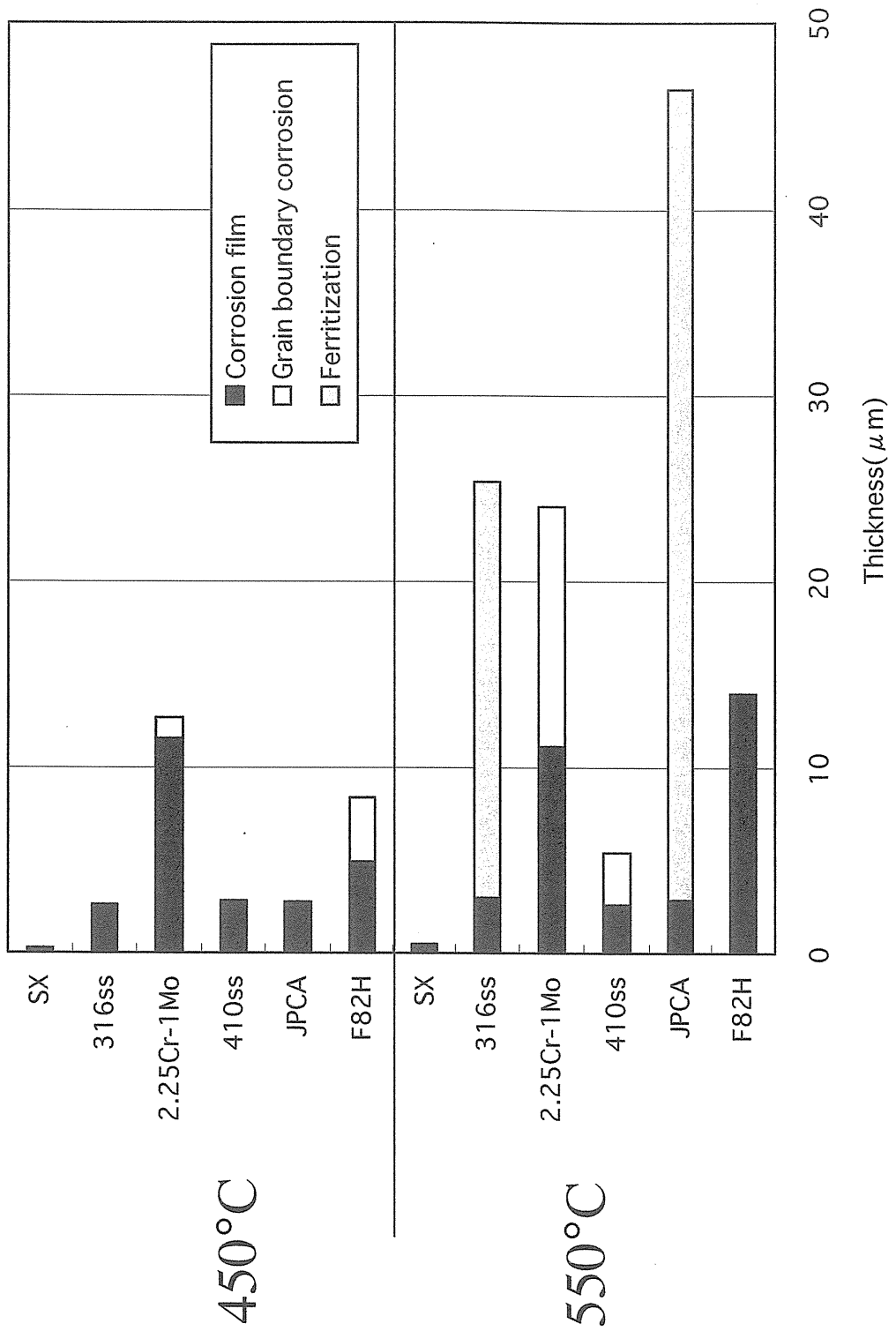

Fig.25 Thickness of corrosion film, grain boundary corrosion, ferritization and total corrosion depth of several steels.

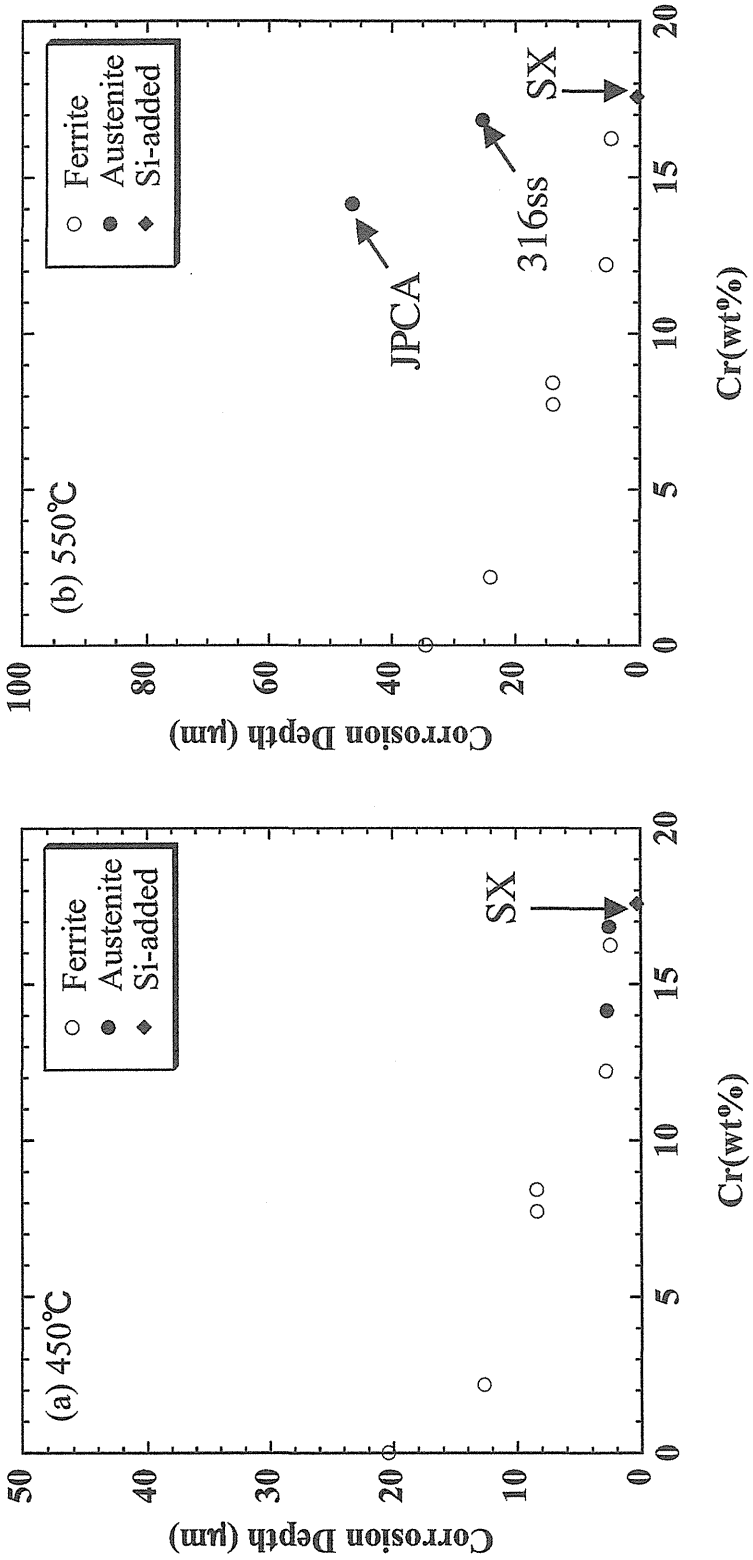

Fig.26 Relationship between corrosion depth and Cr content in steels. The corrosion test was conducted in liquid Pb-Bi at (a)450℃ and (b)550℃, respectively.

This is a blank page.

国際単位系 (SI) と換算表

表 1　SI 基本単位および補助単位

量	名称	記号
長さ	メートル	m
質量	キログラム	kg
時間	秒	s
電流	アンペア	A
熱力学温度	ケルビン	K
物質量	モル	mol
光度	カンデラ	cd
平面角	ラジアン	rad
立体角	ステラジアン	sr

表 2　SI と併用される単位

名称	記号
分，時，日	min，h，d
度，分，秒	°，′，″
リットル	l，L
トン	t
電子ボルト	eV
原子質量単位	u

$1\ \mathrm{eV} = 1.60218 \times 10^{-19}\ \mathrm{J}$

$1\ \mathrm{u} = 1.66054 \times 10^{-27}\ \mathrm{kg}$

表 5　SI 接頭語

倍数	接頭語	記号
10^{18}	エクサ	E
10^{15}	ペタ	P
10^{12}	テラ	T
10^{9}	ギガ	G
10^{6}	メガ	M
10^{3}	キロ	k
10^{2}	ヘクト	h
10^{1}	デカ	da
10^{-1}	デシ	d
10^{-2}	センチ	c
10^{-3}	ミリ	m
10^{-6}	マイクロ	μ
10^{-9}	ナノ	n
10^{-12}	ピコ	p
10^{-15}	フェムト	f
10^{-18}	アト	a

表 3　固有の名称をもつ SI 組立単位

量	名称	記号	他の SI 単位による表現
周波数	ヘルツ	Hz	s^{-1}
力	ニュートン	N	$m \cdot kg/s^2$
圧力，応力	パスカル	Pa	N/m^2
エネルギー，仕事，熱量	ジュール	J	N·m
工率，放射束	ワット	W	J/s
電気量，電荷	クーロン	C	A·s
電位，電圧，起電力	ボルト	V	W/A
静電容量	ファラド	F	C/V
電気抵抗	オーム	Ω	V/A
コンダクタンス	ジーメンス	S	A/V
磁束	ウェーバ	Wb	V·s
磁束密度	テスラ	T	Wb/m^2
インダクタンス	ヘンリー	H	Wb/A
セルシウス温度	セルシウス度	℃	
光束	ルーメン	lm	cd·sr
照度	ルクス	lx	lm/m^2
放射能	ベクレル	Bq	s^{-1}
吸収線量	グレイ	Gy	J/kg
線量当量	シーベルト	Sv	J/kg

表 4　SI と共に暫定的に維持される単位

名称	記号
オングストローム	Å
バーン	b
バール	bar
ガル	Gal
キュリー	Ci
レントゲン	R
ラド	rad
レム	rem

$1\ \text{Å} = 0.1\ \mathrm{nm} = 10^{-10}\ \mathrm{m}$

$1\ \mathrm{b} = 100\ \mathrm{fm}^2 = 10^{-28}\ \mathrm{m}^2$

$1\ \mathrm{bar} = 0.1\ \mathrm{MPa} = 10^5\ \mathrm{Pa}$

$1\ \mathrm{Gal} = 1\ \mathrm{cm/s}^2 = 10^{-2}\ \mathrm{m/s}^2$

$1\ \mathrm{Ci} = 3.7 \times 10^{10}\ \mathrm{Bq}$

$1\ \mathrm{R} = 2.58 \times 10^{-4}\ \mathrm{C/kg}$

$1\ \mathrm{rad} = 1\ \mathrm{cGy} = 10^{-2}\ \mathrm{Gy}$

$1\ \mathrm{rem} = 1\ \mathrm{cSv} = 10^{-2}\ \mathrm{Sv}$

（注）

1. 表 1 ― 5 は「国際単位系」第 5 版，国際度量衡局 1985 年刊行による。ただし，1 eV および 1 u の値は CODATA の 1986 年推奨値によった。
2. 表 4 には海里，ノット，アール，ヘクタールも含まれているが日常の単位なのでここでは省略した。
3. bar は，JIS では流体の圧力を表わす場合に限り表 2 のカテゴリーに分類されている。
4. EC 閣僚理事会指令では bar，barn および「血圧の単位」mmHg を表 2 のカテゴリーに入れている。

換　算　表

力	N(=10^5dyn)	kgf	lbf
	1	0.101972	0.224809
	9.80665	1	2.20462
	4.44822	0.453592	1

粘　度　$1\ \mathrm{Pa \cdot s (N \cdot s/m^2)} = 10\ \mathrm{P}$（ポアズ）$(\mathrm{g/(cm \cdot s)})$

動粘度　$1\ \mathrm{m^2/s} = 10^4\ \mathrm{St}$（ストークス）$(\mathrm{cm^2/s})$

圧力	MPa(=10 bar)	kgf/cm²	atm	mmHg(Torr)	lbf/in²(psi)
	1	10.1972	9.86923	7.50062×10^3	145.038
	0.0980665	1	0.967841	735.559	14.2233
	0.101325	1.03323	1	760	14.6959
	1.33322×10^{-4}	1.35951×10^{-3}	1.31579×10^{-3}	1	1.93368×10^{-2}
	6.89476×10^{-3}	7.03070×10^{-2}	6.80460×10^{-2}	51.7149	1

エネルギー・仕事・熱量	J(=10^7erg)	kgf·m	kW·h	cal(計量法)	Btu	ft·lbf	eV
	1	0.101972	2.77778×10^{-7}	0.238889	9.47813×10^{-4}	0.737562	6.24150×10^{18}
	9.80665	1	2.72407×10^{-6}	2.34270	9.29487×10^{-3}	7.23301	6.12082×10^{19}
	3.6×10^6	3.67098×10^5	1	8.59999×10^5	3412.13	2.65522×10^6	2.24694×10^{25}
	4.18605	0.426858	1.16279×10^{-6}	1	3.96759×10^{-3}	3.08747	2.61272×10^{19}
	1055.06	107.586	2.93072×10^{-4}	252.042	1	778.172	6.58515×10^{21}
	1.35582	0.138255	3.76616×10^{-7}	0.323890	1.28506×10^{-3}	1	8.46233×10^{18}
	1.60218×10^{-19}	1.63377×10^{-20}	4.45050×10^{-26}	3.82743×10^{-20}	1.51857×10^{-22}	1.18171×10^{-19}	1

1 cal = 4.18605 J（計量法）
= 4.184 J（熱化学）
= 4.1855 J（15 °C）
= 4.1868 J（国際蒸気表）

仕事率　1 PS（仏馬力）
= 75 kgf·m/s
= 735.499 W

放射能	Bq	Ci
	1	2.70270×10^{-11}
	3.7×10^{10}	1

吸収線量	Gy	rad
	1	100
	0.01	1

照射線量	C/kg	R
	1	3876
	2.58×10^{-4}	1

線量当量	Sv	rem
	1	100
	0.01	1

（86 年 12 月 26 日現在）

Corrosion Behavior of Austenitic and Ferritic/Martensitic Steels in Oxygen-saturated Liquid Pb-Bi Eutectic at 450℃ and 550℃

古紙配合率100%
白色度70%の再生紙を使用しています